Tome 17 *Février 1979* Numéro 1

うみ

La mer

昭和 54 年 2 月

日 仏 海 洋 学 会

La Société franco-japonaise
d'océanographie
Tokyo, Japon

日 仏 海 洋 学 会

編 集 委 員 会

投　稿　規　定

1. 報文の投稿者は本会会員に限る。
2. 原稿は簡潔にわかりやすく書き，図表を含めて印刷ページで**12ページ以内**を原則とする。原稿（**正1通，副1通**）は，（〒101）東京都千代田区神田駿河台2-3　日仏会館内　日仏海洋学会編集委員会宛に送ること。
3. 編集委員会は，事情により原稿の字句の加除訂正を行うことがある。
4. 論文（欧文，和文とも）には必ず約200語の欧文（原則として仏文）の要旨をつけること。欧文論文には欧文の要旨のほかに必ず約500字の和文の要旨をつけること。
5. 図及び表は必要なもののみに限る。図はそのまま版下になるように縮尺を考慮して鮮明に黒インクで書き，論文の図及び表には必ず英文（又は仏文）の説明をつけること。
6. 初校は原則として著者が行う。
7. 報文には1編につき50部の別刷を無料で著者に進呈する。これ以上の部数に対しては，実費（送料を含む）を著者が負担する。

RECOMMANDATIONS A L'USAGE DES AUTEURS

1. Les auteurs doivent être des Membres de la Société franco-japonaise d'océanographie.
2. Les notes ne peuvent dépasser douze pages. Les manuscrits à deux exemplaires, dactylographiés sur papier fort, doivent être envoyés au Comité de rédaction de la Société franco-japonaise d'océanographie, c/o Maison franco-japonaise, 2-3, Kanda Surugadai, Chiyoda-ku, Tokyo, 101 Japon.
3. Le Comité de rédaction se réserve le droit d'apporter, le cas échéant, des modifications mineuses aux manuscrits ainsi que de demander aux auteurs de les corriger.
4. Des résumés en langue japonaise ou langue française sont obligatoires.
5. Les figures au trait seront tracées à l'encre de Chine noire sur papier blanc ou sur calque. Les légendes des figures et des tableaux sont indispensables.
6. Les premières épreuves seront corrigées, en principe, par les auteurs.
7. Un tirage à part des articles en cinquante exemplaires est offert gratuitement aux auteurs. Ceux qui en désirent un plus grand nombre peuvent les faire établir à leurs frais.

La mer (Bulletin de la Société franco-japonaise d' océanographie)
Tome 17, N° 1, pp. 1 à 10, Février 1979

Aerial and Submarine Spectral Solar Energy Distributions and Optical Characteristics of the Waters in the Bering Sea during the Summer*

Kanau MATSUIKE, Yoshihiko NAKAMURA and Masataka HAGA**

Abstract: In the KH-78-3 Cruise of the Tokyo University's Hakuho-Maru for a period from 5th July to 22nd August, 1978, we carried out a series of measurements of aerial and submarine spectral irradiance and optical characteristics of the water in order to evaluate (1) the distribution of insolations attained on the surface and the relation between insolation amounts and weather conditions, (2) the spectral irradiance distribution of visible lights attained on the sea surface, (3) the underwater spectral and total irradiance distribution, and (4) optical characteristics of the water. The results are summarized as follows.

(1) The total insolation attained on the surface of the Bering Sea during the summer is 560 cal/cm^2/day under clear skies and 200 cal/cm^2/day under overcast skies. The ratio of visible light energy to the total insolation is about 40 % and hardly changes with weather conditions. There exists a fairly close relation between the cloud amount and the insolation expressed by $Q=Q_0(1-0.024\,C^{1.4})$ where Q_0 stands for the possible insolation and Q for the actual insolation.

(2) The underwater spectral distribution patterns depend significantly on the location of the station. The different waters observed are evaluated by Jerlov's Optical Classification (1968) as follows: Intermediate Type between Ocean Types II and III in the northern part of the North Pacific Ocean and in the deep sea area of the Bering Sea, Coastal Type 3 in the deep sea area close to the continental shelf and in the continental slope sea area, and Ocean Type III in the continental shelf area.

(3) A high-turbidity water layer having a beam attenuation coefficient of 1.3 to 1.8 m^{-1} is uniformly distributed from the surface to a depth of 20 m, but the attenuation coefficient strikingly decreases in the underlying layer 20 m thick which constitutes a turbidity boundary layer in the deep sea area close to the continental shelf. This boundary layer is considered as a compensation depth. The relative irradiance of the total lights distributed in this depth is 0.3 % of that of the surface water and the underwater irradiance for each spectral light of blue (484 nm), green (572 nm), and amber (681 nm) are 0.5 %, 5.5 % and 0.02 % of each individual irradiance at the surface water, respectively. On the other hand, the turbidity hardly varies with depths in the continental shelf sea area and is rather small from the surface to the deep layer and then, slightly increases in the bottom layer showing a value of 0.3 to 0.4 m^{-1}. The correlation between the turbidity and the amount of suspended matter can be expressed by an equation of $y=0.53\,x+0.14$ where y stands for the beam attenuation coefficient (m^{-1}) and x for the amount of suspended matter (mg/l). The correlation coefficient obtained is 0.85.

1. Introduction

The authors participated in the KH-78-3 Cruise of the Tokyo University's Hakuho-Maru for a period from 5th July to 22nd August, 1978 and conducted a series of observations in order to find the aerial and submarine spectral solar energy distributions and the optical characteristics of the waters in the Bering Sea and in the nothern part of the North Pacific Ocean.

The study presented herein constitutes a part of studies on "productivities of marine life and

* Recieved October 31, 1978
** Tokyo University of Fisheries, Minato-ku, Tokyo, 108 Japan

circulations of substances" in these sea areas well-known as a good fishing ground with high productivity and considered to be the most interesting waters from the point of view of the optical oceanography.

The optical observation data of these areas are scanty. Only presentations by KAWANA (1975) and OTOBE *et al.* (1977) are available. The former examined the vertical and horizontal distributions of beam attenuation coefficients by a submarine turbidity meter (650 nm) and classified the waters of the Bering Sea into four different types. The latter made an optical observation of the underwater irradiance in the Bering Sea using an irradiance meter equipped with a broad band filter (550 nm) and scrutinized the irradiance attenuation coefficient in its relation with the transparency and the volume of suspended matters.

2. Instrument and observation method

(1) Insolation

Measurements of the total and spectral insolation were continuously made at every station by an Eppley actinograph and a spectral actinograph which were installed on a wing near the top of the stern mast and connected to a CDR 12A high sensitive recorder. The sensing unit of the spectral actinograph consists of a collector with five interference filters of 358 nm (band pass of 50 % points 21 nm), 451 nm (10 nm), 538 nm (9 nm), 630 nm (10 nm) and 720 nm (11 nm), each combined with silicon photocells.

(2) Submarine irradiance

Measurements of the underwater spectral irradiance were made at Stas. 3, 4, 6, 8, 11, 14, 21, 25, 28 and 34 by an underwater spectral irradiance meter equipped with eight interference filters of 375 nm (band pass of 50 % points 19.5 nm), 427 nm (11 nm), 484 nm (11 nm), 513 nm (10 nm), 572 nm (12 nm), 622 nm (11 nm), 650 nm (12 nm) and 681 nm (10 nm), and a photo multiplier (R 636).

(3) Beam transmittance

Measurements of the beam transmittance were made at every station by using an XMS in-situ transmissometers (Martek) with blue (wavelength of gravity center: 486 nm) and red (610 nm) filters. The pass length of the instrument is 1 meter.

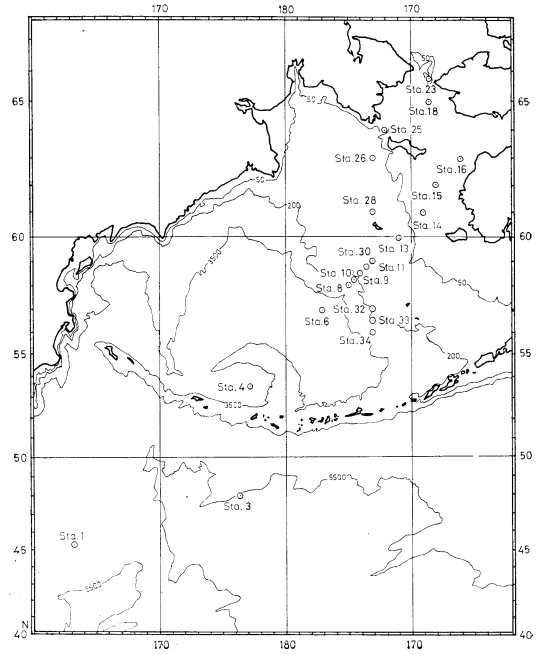

Fig. 1 Map showing the observation stations.

3. Observation stations

Figure 1 shows the locations of the stations. Stations 4, 6, 8, 9 and 34 are located in the sea area deeper than 3,000 m. Stations 10, 11, 13, 26, 28, 30, 32 and 33 are located in the area on the continental slope inclining from a depth of 50 m to 200 m. Stations 14, 15, 16, 18, 23 and 25 are located in the area on the continental shelf 30 m deep.

4. Insolation attained on the sea surface, and relation between climate and insolation

Figure 2 shows the insolation attained on the sea surface in the Bering Sea and the northern part of the North Pacific Ocean from 14th July to 11th August. Numerical figures represent daily insolation estimated by numerical integration.

The insolation is affected considerably by weather conditions. The daily weather distribution during daytime hours measured from sunrise to sunset is shown in Fig. 3. So far as this observation period is concerned, the foggy or/and rainy weather conditions occupy

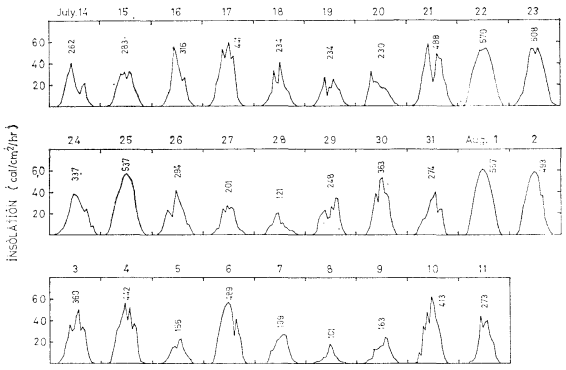

Fig. 2 Insolation during the cruise. Numerical figures represent daily insolation estimated by numerical integration.

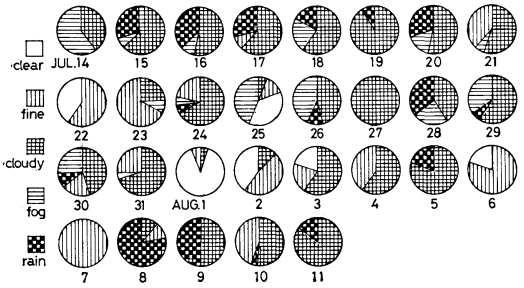

Fig. 3 Distrbution of weather during daytime hours measured from sunrise to sunset in the Bering Sea in summer of 1978.

almost 28% of the total daytime observation hours. Of the remaining 72%, 52% is overcast weather having a cloud amount of more than Grade 8, 12% is partly cloudy or cloudy weather having a cloud amount between Grades 3 and 7, and 8% is fine weather having a cloud amount of less than Grade 2.

When the sunshine is obstructed by clouds only (Fig. 4), there exists a fairly close relation between the cloud amount and the insolation expressed by

$$Q \doteqdot Q_0 (1-0.024\, C^{1.4})$$

Where, "Q_0" stands for "possible insolation", "Q" for "actual insolation", and "C" for "cloud amount". But, no obvious correlation is observed between them under foggy and/or rainy weather.

Figure 5 exhibits a typical example showing how the daily insolation varies with time under

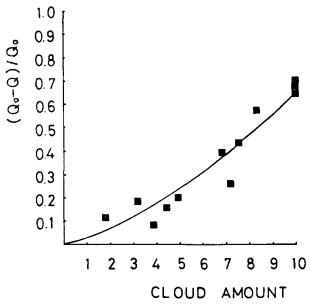

Fig. 4 Relation between the reduction ratio of insolation, $(Q_0-Q)/Q_0$, and cloud amount when sunshine obscured only by clouds.
Q_0: Possible insolation
Q : Actual insolation

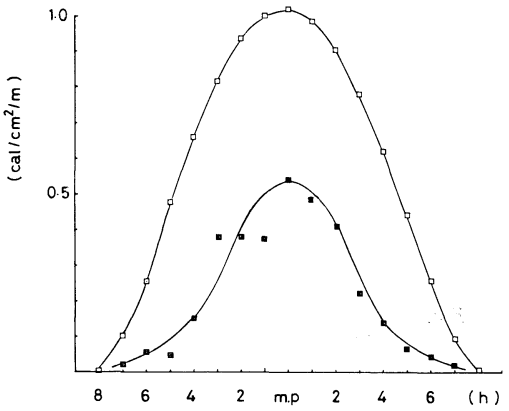

Fig. 5 Insolation during daytime hours measured from sunrise to sunset under clear skies on Aug. 1 and overcast skies on July 27.

each of clear and overcast weather conditions. Data used as a typical example of clear weather was obtained from measurements conducted on 1st August at Lat. 58°N and Long. 153°W, while data of overcast weather was obtained on 27th July at Lat. 61°N and Long. 173°W.

The graph shows the daily insolation to be 560 cal/cm²/day under clear skies, which coincides with the Matsuike's (1970) calculated result of the possible insolation. In contrast, the daily insolation under overcast skies is 200 cal/cm²/day which equals about 36% of the insolation under clear skies.

5. Spectral distribution of insolation

Figures 6-1 and 2 show the spectral insolation in a range of visible lights under clear and

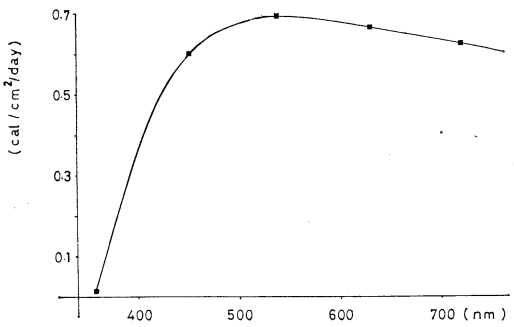

Fig. 6-1 Spectral insolation under clear skies on Aug. 1.

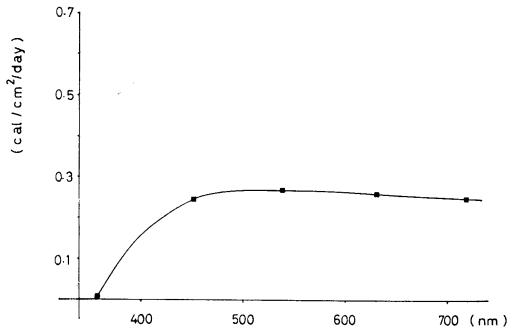

Fig. 6-2 Spectral insolation under overcast skies on July 27.

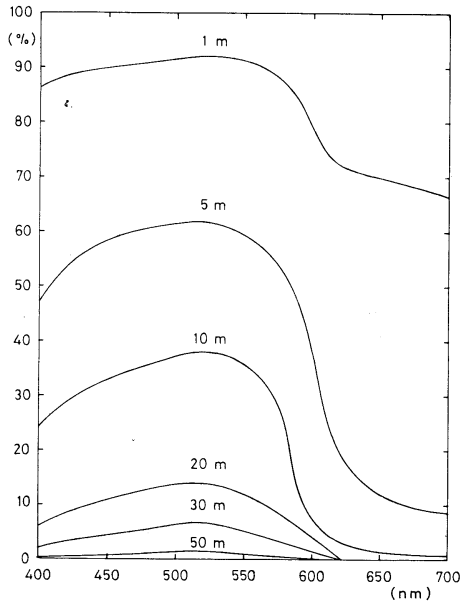

Fig. 7 Underwater spectral distribution of downward irradiance at Sta. 3.

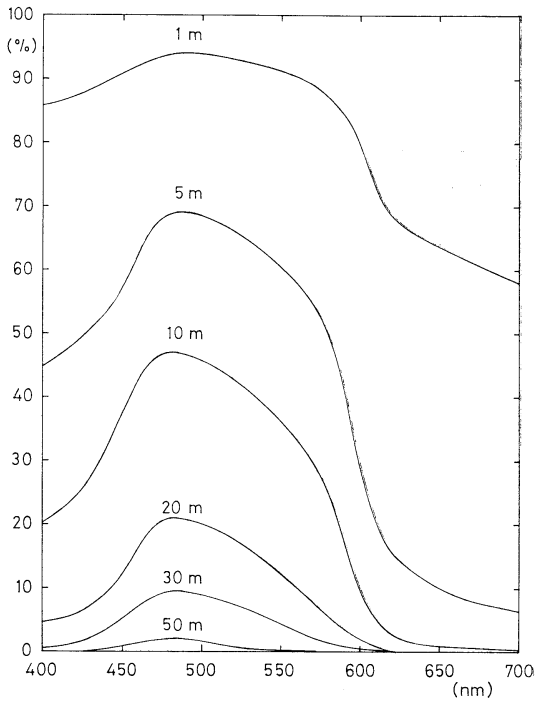

Fig. 8-1 Underwater spectral distribution of downward irradiance at Sta. 4.

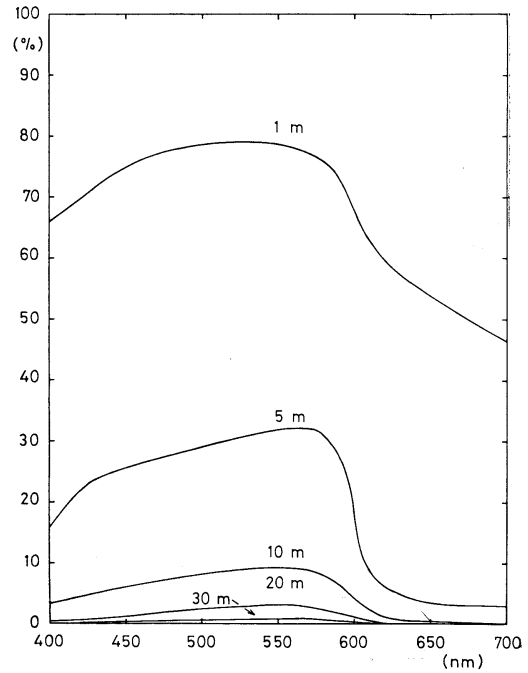

Fig. 8-2 Underwater spectral distribution of downward irradiance at Sta. 6.

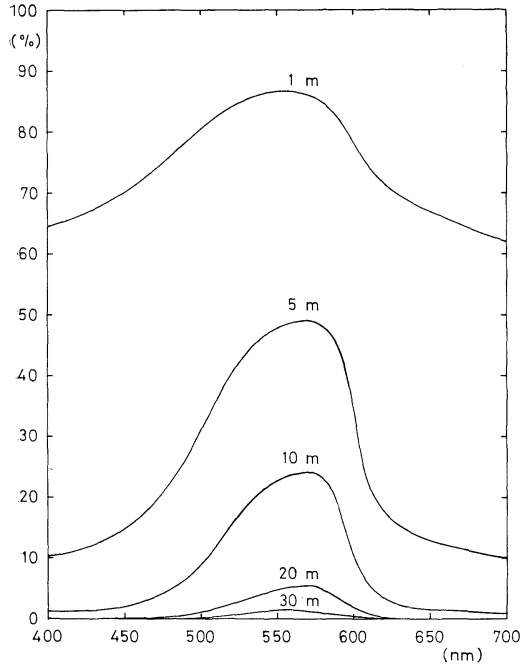

Fig. 8-3 Underwater spectral distribution of downward irradiance at Sta. 8.

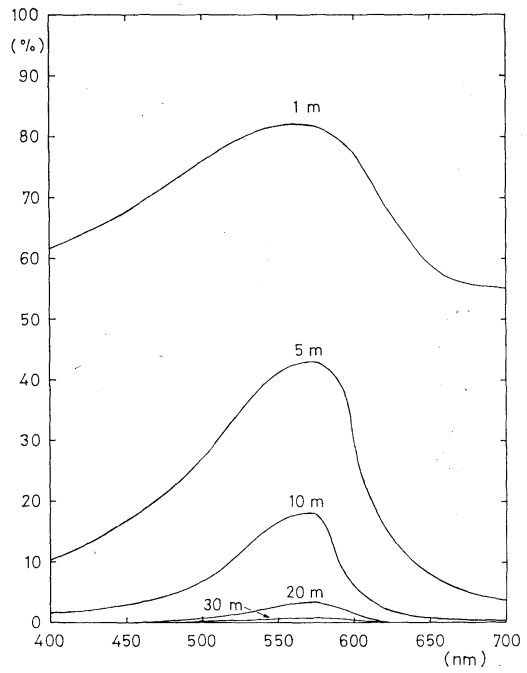

Fig. 9 Underwater spectral distribution of downward irradiance at Sta. 11.

overcast skies.

Energy of the visible light obtained from the graph is 200 cal/cm^2/day under clear skies while it is 80 cal/cm^2/day under overcast skies. The ratio of the visible light energy to the total insolation is about 40 %, and hardly changes with weather conditions.

6. Distribution of underwater spectral and total irradiance

Figure 7 shows the distribution of underwater spectral irradiance at Sta. 3 in the northern part of North Pacific Ocean. Figs. 8-1, 2 and 3 show the distributions at Stas. 4, 6 and 8 in the deep sea area of the Bering Sea. Fig. 9 shows the distribution at Sta. 11 in the continental slope area and Fig. 10 the distribution at Sta. 14 in the continental shelf area.

The spectral irradiance attenuation coefficients of different wavelengths in the upper layer are listed in Table 1.

According to Jerlov's Optical Classification (JERLOV 1968), the waters mentioned above are Intermediate Type between Ocean Types II

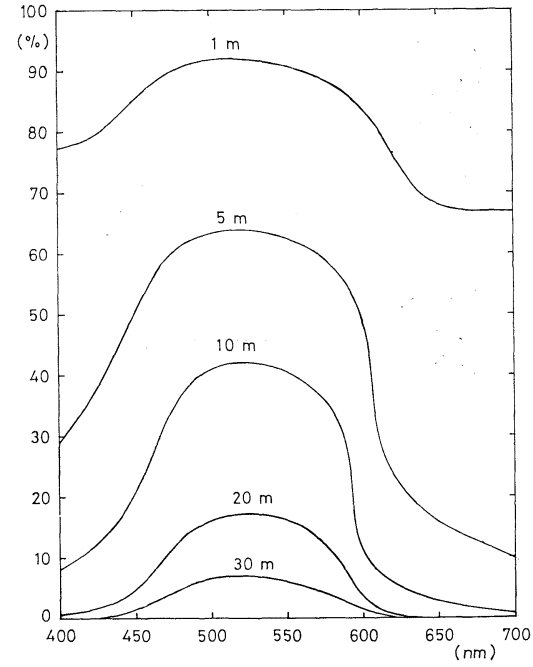

Fig. 10 Underwater spectral distribution of downward irradiance at Sta. 14.

Table 1. Spectral irradiance attenuation coefficients in the upper layer

	375nm	427nm	484nm	513nm	572nm	622nm	650nm	681nm
Sta. 3 0-20 m	0.23	0.12	0.10	0.098	0.12	0.36	0.43	0.49
Sta. 4 0-30 m	0.16	0.14	0.078	0.098	0.13	0.38	0.42	0.53
Sta. 6 0-10 m	0.39	0.30	0.26	0.27	0.24	0.45	0.50	0.56
Sta. 8 0-20 m	0.36	0.36	0.26	0.20	0.15	0.35	0.41	0.43
Sta. 11 0-10 m	0.36	0.39	0.30	0.24	0.17	0.39	0.49	0.54
Sta. 14 0-10 m	0.29	0.20	0.096	0.087	0.10	0.29	0.36	0.42

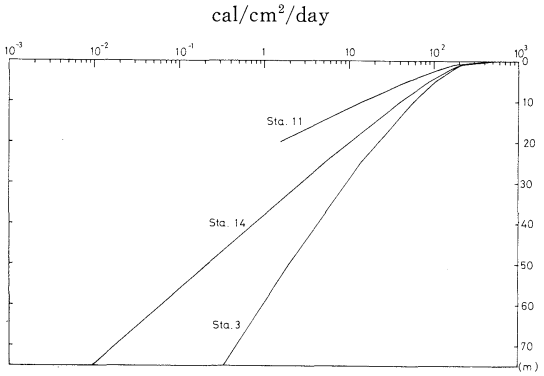

Fig. 11-1 Distribution of underwater solar energy in fine weather.

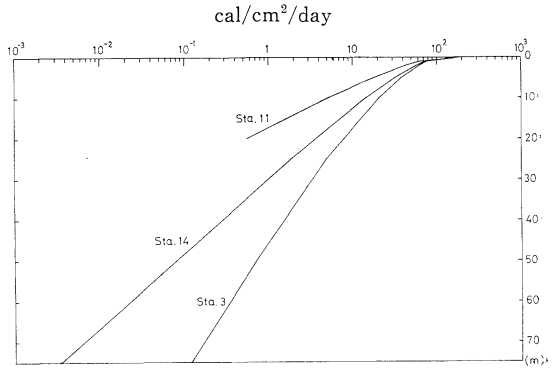

Fig. 11-2 distribution of underwater solar energy in overcast weather.

and III at Sta. 3 in the northern part of the North Pacific Ocean and at Sta. 4 in the deep sea area in the Bering Sea, Coastal Type 3 at Stas. 6 and 8 in the deep sea area in the Bering Sea and Sta. 11 in the continental slope sea area in the Bering Sea, and Ocean Type III at Sta. 14 in the continental shelf sea area.

Based on the insolation amounts attained on the sea surface and underwater spectral transmittance, underwater solar energies under different weather conditions are calculated, as shown in Figs. 11-1 and 2, using solar energy reflection rates given by COX and MUNK (1956).

As seen in Figs. 11-1 and 2, the underwater solar energies in these areas are fairly different from each other depending on the location of the area, even if the same insolation amount attains on the sea surface. For example, the amount of underwater solar energy at a depth of 10 m at Sta. 11 is only 1/3 of that at Sta. 3.

It is easily understood from Figs. 8, 9 and 10 that the transmittance peak appears for a wavelength of 480 nm at Sta. 4 located in the south edge of the Bering Sea, while the corresponding peak shifts to 570 nm at Sta. 8 located close to the continental shelf. This tendency is exhibited more clearly at Sta. 11 located in the continental slope water area. At Sta. 14 in the continental shelf sea area, however, the light transmittance peak goes back to 520 nm. The shift of the transmittance peak is attributed to the fact that the spectral light attenuation is large for short waves.

BURT (1958) and KALLE (1966) clarify that the underwater light absorption by organic suspended and/or dissolved organic matters increases as the wavelengths of underwater spectral light become shorter. According to them, the difference in the spectral distribution between these areas indicates that organic suspended and/or dissolved organic matters are very abundant in the sea area close to the continental shelf but not abundant in the continental shelf sea area.

7. Turbidity (Beam attenuation coefficient)

Figures 12, 13-1, 2, 3, 14 and 15 show the vertical distributions of beam attenuation coefficients at Sta. 3 in the northern part of the North Pacific Ocean, at Stas. 4, 6 and 8 in the

deep sea area in the Bering Sea, at Sta. 11 in the continental slope sea area, and at Sta. 14 in the continental shelf sea area, respectively.

The aforementioned hypothesis on the amount of organic matters built up in terms of the underwater spectral distribution is verified as follows, when reexamined in terms of the underwater turbidity distribution. At Sta. 6 in the deep sea area close to the continental shelf, the high-turbidity of 1.3 m^{-1} is uniformly distributed in the whole layer from the surface down to a depth of about 20 m, but the turbidity decreases so strikingly in the underlying layer about 20 m thick that a sharp boundary layer is formed. There is a very clear water of 0.1 m^{-1} underneath this boundary layer. Similar tur-

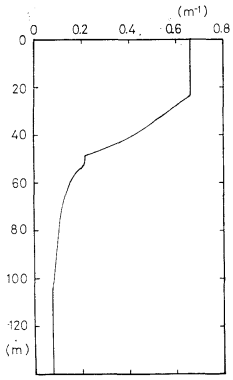

Fig. 12 Depth profile of beam attenuation coefficient at Sta. 3.

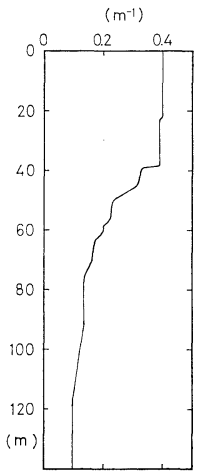

Fig. 13-1 Depth profile of beam attenuation coefficient at Sta. 4.

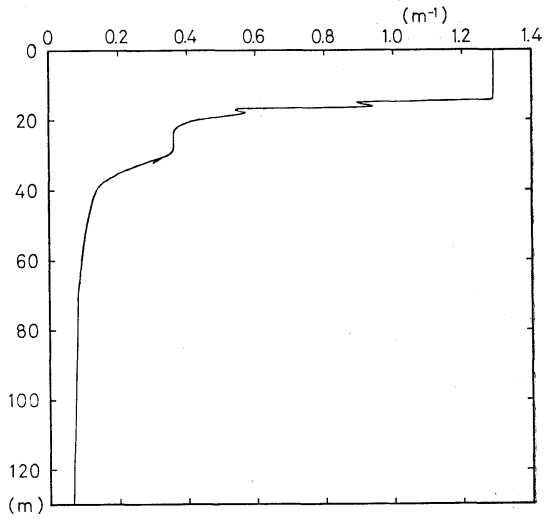

Fig. 13-2 Depth profile of beam attenuation coefficient at Sta. 6.

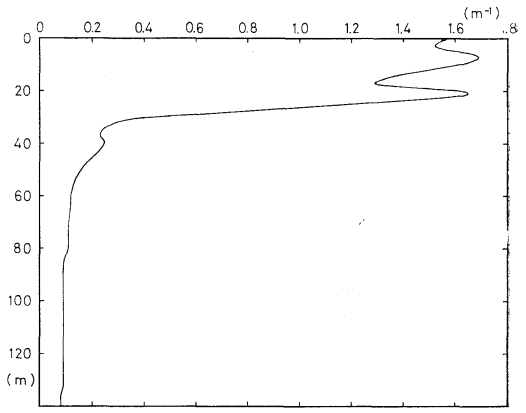

Fig. 13-3 Depth profile of beam attenuation coefficient at Sta. 8.

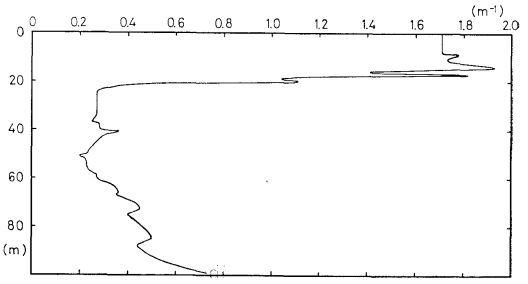

Fig. 14 Depth profile of beam attenuation coefficient at Sta. 11.

bidity boundary layers are also present at Sta. 8 near the continental shelf and at Sta. 11 on the continental slope. At at Sta. 14 located in the continental shelf sea area, however, the turbidity shows a small value of 0.35 m^{-1} and slightly increases with depths.

There is a close relation between the beam attenuation coefficient and the amount of the suspended matters. Its correlation coefficient is more than 0.85 (Fig. 16). This relation can be expressed by

$$y=0.53x+0.14,$$

where y is the beam attenuation coefficient (m^{-1}) and x is the amount of suspended matter (mg/l). It might be parenthetically remarked that the amount of suspended matter was measured by E. TANOUE of Nagoya University.

The above discussion allows to confirm that the high turbidity in the sea area close to the continental shelf is mainly caused by organic suspended matters and that the water abundant in organic suspended matters is limited from the surface down to a depth of about 20 m, whereas the organic suspended matter is not abundant in the continental shelf sea area, the amount being almost constant from the surface down to the bottom.

The boundary layer about 20 m deep between the high and low turbidity waters is considered as a compensation depth. The underwater irradiance of the total light in this layer is 0.3 % of that in the surface water. The underwater irradiance for each spectral light of blue (484 nm), green (572 nm) and amber (681 nm) is 0.5 %, 5.5 % and 0.02 % of each individual irradiance at the surface water, respectively.

To find possible causes of high productivity in the sea area close to the continental slope,

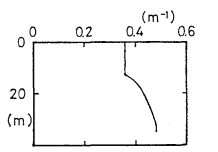

Fig. 15 Depth profile of beam attenuation coefficient at Sta. 14.

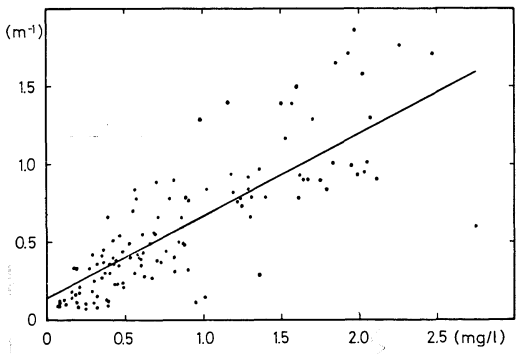

Fig. 16 Relation between the beam attenuation coefficient and the amount of suspended matters.

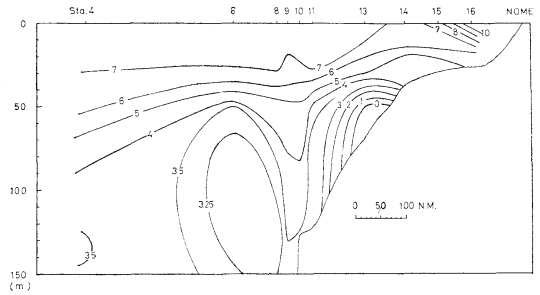

Fig. 17 Vertical profile of water temperature (°C) from Sta. 4 to Sta. 16.

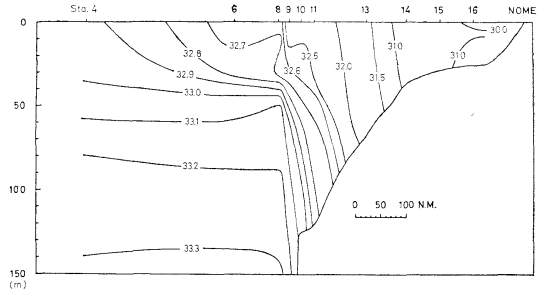

Fig. 18 Vertical profile of salinity (‰) from Sta. 4 to Sta. 16.

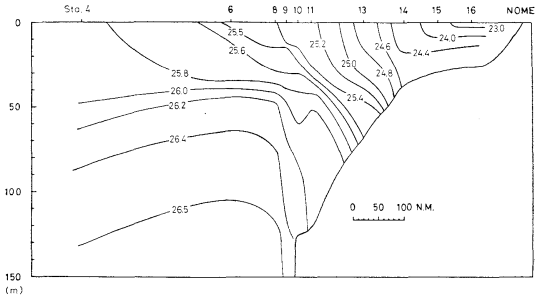

Fig. 19 Vertcal profile of density (σ_t) from Sta. 4 to Sta. 16.

temperature, salinity and density distributions are shown in Figs. 17, 18 and 19, respectively (Preliminary Report of the Hakuho-Maru Cruise KH-78-3, Ocean Research Institute, University of Tokyo, 1979).

It is worthwhile to mention here that the sea area close to the continental shelf is enriched by the effect of low-salinity coastal water to be a high-productive area. On the contrary, the continental shelf sea area is not abundant in organic suspended matters, which should be interpreted as follows.

The coastal water is hardly replaced with the external off-shore waters because of its shallowness, so that the nutritive salts are not sufficiently supplemented after used up for the high production in spring, and then poor productivity of marine life is brought about.

In other words, the high productive season had come to a termination in those days when the observation was conducted in this sea area, and the propagation of marine life was under control due to the phenomenon called "exhaustion."

It is worthwhile to notice that the depth of the turbidity boundary layer does not agree with that of the seasonal thermocline, but is located above it.

It should be useful to compare the optical characteristics of the waters in the Bering Sea with those in other oceans for more detailed review of the optical structures of different waters in relation to the distributions of temperatures, salinities and densities. These problems will be discussed in other occasions.

Acknowledgements

We wish to thank Prof. A. HATTORI and scientists aboard the KH-78-3 Cruise and Captain I. Tadama, the officers and crew members of the R/V Hakuho-Maru for their cooperation.

References

BURT, W.V. (1958): Selective transmission of light in tropical Pacific waters. Deep-Sea Res., **5**, 51-61.

COX, C. and W. MUNK (1956): Slopes of the sea surface deduced from photographs of sun glitter. Bull. Scripps Inst. Oceanogr. Univ. Calif., **6**, 401-488.

JERLOV, N.G. (1968): Optical Oceanography. Elsevier Oceanography Series, 5. Elsevier Publishing Co. Amsterdam, 118-123.

KALLE, K. (1966): The problem of the Gelbstoff in sea. Oceanogr. Mar. Biol. Ann. Rev, **4**, 91-104.

KAWANA, K. (1975): Turbidity distribution of the Bering Sea in the summer. Bull. Fac. Fish. Hokkaido Univ., **26**, 73-86.

MATSUIKE, K. (1969): The optical characteristics of the water in three oceans. (Part-3) The distribution of solar energy reached to and penetrated in the water of the Antarctic Ocean in the summer and its comparison to other oceans. J. Oceanog. Soc. Japan, **25**, 81-90.

MATSUIKE, K., T. MORINAGA and T. SASAKI (1970): The optical characteristics of the water in the three oceans. (Part-4) An attempt to the approximate figures of seasonal solar energy reached to and penetrated in the water of the three oceans. J. Oceanog. Soc. Japan, **26**, 52-60.

MATSUIKE, K. (1963): A study on optical nature in oceanic waters. La mer, **11**, 1-44.

MATSUIKE, K. and T. MORINAGA (1977): Beam attenuation and particle-size distribution in the Kuroshio area. La mer, **15**, 82-93.

OHTANI, K. (1969): On the oceanographic structure and the ice formation on the continental shelf in the eastern Bering Sea. Bull. Fac. Fish. Hokkaido Univ., **20**, 94-117.

OTOBE, H., T. NAKAI and A. HATTORI (1977): Underwater irradiance and Secchi disk depth in the Bering Sea and the northern North Pacific in summer. Marine Science Communications, **3**, 255-270.

夏季ベーリング海における天空および海中の分光太陽エネルギー分布と海水の光学的性質

松生　洽，中村善彦，芳賀正隆

要旨: 1978年7月5日から8月22日の間，東京大学白鳳丸 KH-78-3 次航海（ベーリング海，チャクチ海，北部北太平洋における生物活動と物質循環に関する研究）に参加して，天空および海中の分光照度や海中の濁度（Beam attenuation coefficient）を測定した。これに基づいて，(1) 海面日射量および日射量と天候との関係，(2) 可視部の海面分光照度分布，(3) 海中分光照度分布および海中太陽エネルギー量，(4) 海中濁度分布を求めた。

その結果は次のように要約される。

1. 夏季ベーリング海における海面日射量は晴天日で約 560 cal/cm^2/day，曇天日で約 200 cal/cm^2/day である。可視部エネルギー量の全日射量に占める割合は約 40 % で天候による差は小さい。雲と日射量との関係は次のように表わされる。 $Q=Q_0(1-0.024\,C^{1.4})$，Q_0: 可能日射量（晴天日の日射量），Q: 海面日射量。

2. 海中分光照度分布は観測点の位置によって顕著に異なる。JERLOV (1968) の Optical classification を引用すると北太平洋北部やベーリング海入口付近の海域は Ocean type II と III の中間，大陸棚に接近した海域では Coastal type 3，大陸棚上の海域は Ocean type III に該当する。

3. ベーリング海の大陸棚に近接した海域では上層に高濁度層が存在する（1.3～1.8 m^{-1}）。この高濁度層の厚さは表層から約 20 m 深までであり，それ以深は急激に濁度が減少する。この濁度の境界層は Compensation depth と考えられる。この深さの相対照度は全光で表面の約 0.3 % であり，さらに波長別に見ると Blue (484 nm) で 0.5 %，Green (572 nm) で 5.5 %，Amber (681 nm) で 0.02 % となる。一方大陸棚上の海域では，上層から海底までほとんど変化がなく，むしろ海底近くで増大する傾向がある（0.3～0.4 m^{-1}）。濁度と懸濁物量との関係は次式で表わされ，相関係数は 0.85 である。$y=0.53\,x+0.14$，y: Beam attenuation coefficient (m^{-1})，x: 懸濁物量 (mg/l)。

以上の光学的結果に水温および塩分の分布を加えて考察すると，大陸棚に近接した海域の上層における高生産性は塩分量の少ない沿岸水の張出しによるものであり，大陸棚上の低生産性は海水の交換が悪いために春先における高生産時に使われた栄養塩の補給がなされないことによるものと推察される。

La mer (Bulletin de la Société franco-japonaise d'océanographie)
Tome 17, N° 1, pp. 11 à 17, Février 1979

Accumulation of Ni from the Environmental Sea Water and Sediments by Various Marine Organisms*

Akira KURATA**, Yoichi YOSHIDA** and Fumio TAGUCHI***

Abstract: The accumulation of Ni was studied in the tissues of various marine organisms collected from the Sea of Aso which has long received the Ni pollution. The accumulation of Ni in different kinds of organisms collected from the Ni-polluted area was compared with that of organisms collected from the unpolluted area. In the Ni-polluted areas, Ni was accumulated extremely in several kinds of seaweeds and shellfishes, and also accumulated appreciably even in the tissues of a few kinds of fishes. The accumulation pattern of Ni in seaweeds was very different. The highest level of concentration factor of Ni was observed in *Enteromorpha prolifera* and *Grateloupia filicina*, and it was 1750 and 860, respectively. A relatively high concentration factor of Ni was also observed in a seagrass, *Zostera marina*, and it was 1690. An appreciable amount of Ni was accumulated in *Tapes* (*Amygdala*) *japonica* which is the most famous and important fish-catch in these areas, but the concentration factor was not so high.

1. Introduction

Previously, we have reported the distribution of Ni-tolerant bacteria in sea water and sediments in the Sea of Aso which has long received industrial waste water containing Ni from a metallurgical factory (KURATA *et al.*, 1977). It is supposed that various coastal organisms including seaweeds, seagrasses, invertebrates and vertebrates have also received waste water containing Ni and have accumulated Ni in their tissues from the environmental waste water and sediments in this area.

NISHIKAWA (1969) reported the acute lethal toxicity of Ni for carps and GILMAN (1962) reported that the cancer was caused by the intramuscular injection of Ni in rats. The distribution of heavy metals, such as Cd, Hg, Cu, Zn and Pb, in the coastal sea waters and sediments and the accumulation of such metals from sea water by various marine invertebrates have been investigated by many researchers (PHILLIPS, 1976). However, few reports have been published concerned with the trend and degree of Ni accumulation from sea water by various marine organisms and the toxicity of Ni as a pollutant for them in the coastal environments of the sea.

In the present paper we attempted to elucidate the Ni accumulation from the environmental sea water and sediments by various organisms in the coastal areas of the Sea of Aso which has received the Ni pollution from a metallurgical factory and to compare the result with that in an unpolluted area.

2. Materials and methods

(1) Samples of organisms

This study was made with various organisms including netplankton, seaweeds, seagrass, invertebrates and vertebrates collected from the Sea of Aso, Miyazu Bay and Kunda Bay of Kyoto Prefecture. The samples were collected at designated stations shown in Fig. 1 in summer of 1972. The collected samples were immediately chilled and carried to the laboratory and frozen at −20°C till the assay procedure.

(2) Determination of Ni in samples

* Received November 3, 1978
This work was supported by a Grant-in-Aid for Scientific Research (No. 976116) from the Ministry of Education, Science and Culture, Japan.
** Department of Fisheries, Faculty of Agriculture, Kyoto University, Kitashirakawa-Oiwake-cho, Sakyo-ku, Kyoto, 606 Japan
*** Kyoto Senior High School of Fisheries, Joshi, Miyazu City, 626 Japan

Samples were dipped into the artificial sea water and rinsed, dried roughly, and then reduced completely to ashes by heating with nitric acid. Ni contained in the ashes was extracted and determined according to the method described in a previous paper (KURATA, 1974) using an atomic absorption spectrophotometer (Hitachi model 208). For each kind of organism several samples were analyzed and the values obtained were averaged.

(3) Calculation of concentration factor of Ni

Concentration factor of Ni in organisms was calculated according to the formula described by ICHIKAWA (1961).

3. Results and discussion

The data obtained by an atomic absorption

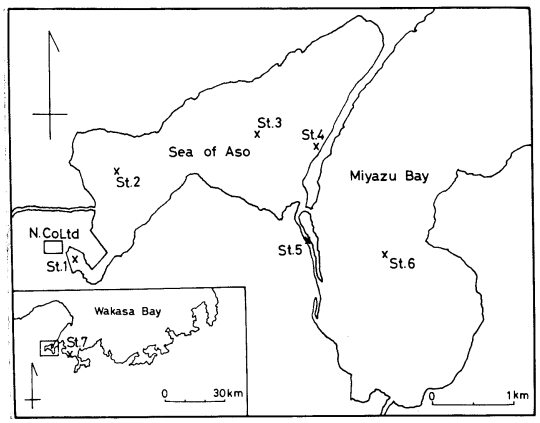

Fig. 1. Location of the sampling stations in the Sea of Aso and Miyazu Bay.

Table 1. The concentrations of Ni in sea water of the investigated area.

Station	Depth (m)	Concentration of Ni ($\mu g/l$)
1	0.5	23.0
2	0.5	17.0
	5	16.0
3	0.5	22.0
	5	13.0
	8	29.0
6	0.5	12.0
	5	14.7
	14	14.0
7	0.5	7.5

Table 2. The concentrations of Ni in sediments of the investigated area.

Station	Core depth (cm)	Concentration of Ni ($\mu g/g$ dry matter)
1	0～ 2	1,890
2	0～ 2	700
	6～ 8	56
	12～14	49
3	0～ 2	630
	6～ 8	53
	12～14	51
6	0～ 2	31
	6～ 8	25
	12～14	20
7	0～ 2	12

Table 3. Comparison of the concentrations of Ni in netplankton and various aquatic organisms collected from the Ni-polluted and unpolluted areas.

Organism	Concentration of Ni ($\mu g/g$ dry matter)			
	Polluted area			Unpolluted area
	St. 4	St. 5	St. 6	St. 7
Netplankton	115	—	63	32
Enteromorpha prolifera	400	—	—	4
Ulva pertusa	8	4	—	3
Grateloupia filicina	88	4	—	3
Sargassum fulvellum	79	—	—	6
Zostera marina	220	80	—	—
Tapes (Amygdala) japonica	56	11	—	4
Mytilus edulis	77	11	—	—
Neanthes diversicolor	57	—	—	6

spectrophotometer for the concentration of Ni in sea water and sediments in the investigated areas are shown in Tables 1 and 2. Stations 1, 2 and 3 were located in the Sea of Aso which has long received industrial waste water containing Ni from a metallurgical factory, and their sediments showed a comparatively higher concentration of Ni than those at Stations 6 and 7. The surface layer of sediments at Station 1 which was located closely near the discharge site of Ni showed an extremely high concentration of Ni. It is said that the concentration of Ni in sea water and sediments in the coastal areas of our country is about several $\mu g/l$ and about 50 $\mu g/g$ dry matter or so, respectively (SUGIMURA, 1972). Judging from the value, it is thought that the concentration of Ni in sea water in Miyazu Bay has been affected to some extent by the Ni discharge from the Sea of Aso. Recently, HUTCHINSON (1974) reported that 5104 $\mu g/g$ dry matter of Ni was contained in heavily polluted soil near a smelter in Canada.

The concentrations of Ni in various marine organisms including netplankton, seaweeds, seagrass and invertebrates are shown in Table 3. The values for the samples collected from the Sea of Aso and Miyazu Bay where sea water has been polluted by Ni are compared with those for the samples from Kunda Bay where water has not been polluted. *Zostera marina* and *Mytilus edulis* could not be collected near Station 6. The concentrations of Ni in the cells of netplankton and other aquatic organisms which were collected from the Ni-polluted areas were relatively high as compared with the samples of the same kinds of organisms which were collected from the Ni-unpolluted area. Ni was accumulated in the cells of the former to the extent of 2.6 to 100 fold as compared with the latter. Ni was accumulated in *Enteromorpha prolifera* in an extremely high concentration. It is supposed that this extremely high level of Ni accumulation in this alga may be due to the fact that this aquatic organism has the relatively large external surface area for its weight comparing with the other organisms. It is also supposed that this alga was probably growing actively in this season and taking up actively various kinds of dissolved nutrients including heavy metals for its growth. Except for *Ulva pertusa*, the Ni accumulation was higher in seaweeds and seagrass than in invertebrates. BRYAN (1973) reported very high level of Ni accumulation in scallops collected from the English Channel near Plymouth; the maximum was about 150 $\mu g/g$ dry tissue of kidney. But, generally the Ni accumulation in scallops ranged from 3 to 110 $\mu g/g$ dry tissue, and it was

Table 4. Comparison of the concentrations of Ni in the tissues of several marine fishes collected from the Ni-polluted and unpolluted areas.

Organism and tissue		Ni content ($\mu g/g$ dry matter)		a/b
		St. 1 [a]	St. 7 [b]	
Acanthogobius flavimanus	Muscle	11.0	2.0	5.5
Tribolodon hakonensis hakonensis	Muscle	6.0	1.0	6.0
Leiognathus equulus	Intestine	490.0	13.3	36.8
	Muscle	11.0	1.3	8.5
Fugu niphobles	Gill	3.0	0.7	4.3
	Muscle	1.4	2.7	0.5
	Bone	7.5	2.7	2.8
Mugil cephalus	Gill	104.0	5.0	20.8
	Muscle	17.0	2.3	7.4
	Bone	20.0	1.3	15.4
Mylio macrocephalus	Gill	21.0	5.3	4.0
	Liver	2.7	2.7	1.0
	Muscle	1.7	1.3	1.3
	Bone	9.0	2.0	4.5

Table 5. The accumulation of Ni in the tissue of several organisms as compared with the other heavy metals content.

Organism (collected from the Ni polluted and unpolluted areas)		Metal content (μg/g dry matter)					
		Ni	Fe	Co	Cu	Pb	Cd
Enteromorpha prolifera	(a)*	400	1650	12	10	6.4	0.1
	(b)**	4	2875	19	5	12.0	0.7
	(a)/(b)	100	0.6	0.6	2.0	0.5	0.1
Grateloupia filicina	(a)	88	2700	8	1	16.0	1.6
	(b)	3	700	14	5	8.0	0.6
	(a)/(b)	29.3	3.9	0.6	0.2	2.0	2.7
Sargassum fulvellum	(a)	79	2400	3	6	6.4	2.4
	(b)	6	1800	3	9	9.0	1.6
	(a)/(b)	13.2	1.3	1.0	0.7	0.7	1.5
Neanthes diversicolor	(a)	57	7000	8	16	9.6	2.4
	(b)	6	4200	3	72	21.0	1.6
	(a)/(b)	9.5	1.7	2.7	0.2	0.5	1.5
Mytilus edulis	(a)	77	559	5	7	4.8	1.2
	(b)	11	110	5	9	6.4	0.6
	(a)/(b)	7.0	5.1	1.0	0.8	0.8	2.0
Mugil cephalus (Gill)	(a)	104	400	6	9	19.2	3.8
	(b)	5	44	3	8	7.1	0.6
	(a)/(b)	20.8	9.1	2.0	1.1	2.7	6.3

* Collected from the Sea of Aso which is the Ni-polluted area.
** Collected from Kunda Bay which is the Ni-unpolluted area.

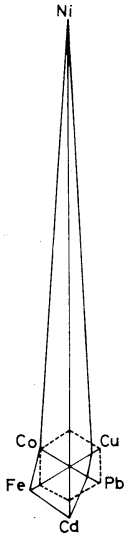

Fig. 2. Relative accumulation of Ni, Cu, Pb, Cd, Fe and Co in *Sargassum fulvellum* collected from the Sea of Aso (solid line) and from Kunda Bay (broken line). Content of the heavy metals in the latter samples are illustrated as hexagon.

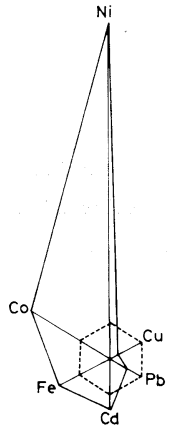

Fig. 3. Relative accumulation of Ni, Cu, Pb, Cd, Fe and Co in *Neanthes diversicolor* cellected from the Sea of Aso (solid line) and from Kunda Bay (broken line). Content of the heavy metals in the latter samples are illustrated as hexagon.

almost the same level as that in *Tapes* (*Amygdala*) *japonica*, *Mytilus edulis* and *Neanthes diversicolor* in the present study. The Ni accumulation in different tissues of several marine fishes collected from the Ni-polluted and unpolluted areas is shown in Table 4. The highest concentration of Ni was observed in the intestines of *Leiognathus equulus*. The concentration of Ni was relatively higher in gills of *Mylio macrocephalus* and *Mugil cephalus* than in the other tissues. The concentration of Ni in various tissues of the fishes collected from the Ni-polluted area was generally higher than that of the fishes collected from the unpolluted area. Much amount of Ni as detected in the gills of *M. cephalus* might be accumulated directly from the environmental sea water of the high concentration of Ni.

The accumulation of Ni was compared with that of other heavy metals in the tissues of several organisms as shown in Table 5. Content of 6 kinds of heavy metals was determined and compared with each other in the tissues of organisms which were collected from the Ni-polluted and the unpolluted areas. In the cases of Co, Cu and Pb, there were no great differences between the concentration of heavy metals in the tissue of different kinds of organisms collected from the polluted area and that of the unpolluted area. While the concentration of Ni in the tissue of all kinds of organisms obtained from the polluted area was considerably higher than that of the unpolluted area, and 100 fold Ni was accumulated in the tissue of *E. prolifera* collected from the polluted area as compared with that from the unpolluted area. This suggests undoubtedly that the pollution of only Ni discharged from a metallurgical factory has long been progressing in the polluted area and that Ni has been taken up and accumulated obviously in the tissue of various marine organisms more or less under such environmental circumstances in the area. The Ni accumulation in the cells of *S. fulvellum* and *N. diversicolor* is shown more clearly in Figs. 2 and 3 in comparison with the other kinds of heavy metals.

Biological accumulation of Ni by various marine organisms collected from the Ni-polluted area is shown in Table 6 as the concentration factor. The concentration factor ranged from 90 to 1750 in these organisms. It was considerably high in *E. prolifera* and *Z. marina*. In the Ni-polluted area, the concentration factor of Ni of seaweeds and shellfishes, such as *E. prolifera*, *Grateloupia filicina*, *M. edulis* and *T.* (*Amygdala*) *japonica*, was higher than that of fishes, such as *M. cephalus* and *Acanthogobius flavimanus*. This tendency of Ni accumulation in different kinds of organisms in this area suggests that direct uptake of Ni from the environmental sea water and accumulation in the tissue of these organisms like netplankton, seaweeds, seagrass and shellfishes are more active than the accumulation in the tissue of

Table 6. Concentration factor of Ni in various marine organisms collected from the Sea of Aso.

Organism and tissue	Ni content		Concentration factor*
	(μg/g dry matter)	(μg/g wet matter)	
Enteromorpha prolifera	400	32.0	1750
Zostera marina	200	31.0	1690
Mytilus edulis	77	17.9	980
Grateloupia filicina	88	15.7	860
Tapes (*Amygdala*) *japonica*	56	15.6	850
Sargassum fulvellum	79	14.9	810
Netplankton	115	11.5	630
Neanthes diversicolor	57	6.3	340
Mugil cephalus (Muscle)	17	4.1	220
Acanthogobius flavimanus (Muscle)	11	2.3	130
Ulva pertusa	8	1.6	90

* The averaged value of Ni concentration of sea water in the Sea of Aso was 18.3 mμg/m*l*, which was used for the calculation.

fishes which seem to take up and accumulate Ni mainly through the food chain. PENTREATH (1973) reported that the concentration factor of Co in stomach and digestive gland of *M. edulis* was 10,500. But the concentration factor of Ni in marine organisms was not demonstrated in his report. While BROOKS *et al.* (1974) reported the concentration factor of Ni of the terrestrial plants in New Caledonia and it was at very low level. The concentration factor of heavy metals in marine organisms must be different both with the kind of metals and with the kind of organisms under varying environmental circumstances. It was reported by GILMAN (1962) that a single intramuscular injection of Ni sulfide and Ni oxide induced primary rhabdomyosarcoma and primary fibrosarcoma in rats. However, we could not find any symptom of sarcoma in the tissues of fishes which were collected from the Ni-polluted areas and accumulated a relatively high level of Ni in their tissues. The concentration factor of Ni in *T.* (*Amygdala*) *japonica*, one of the most important and famous fish-catch in the area concerned, was not so high.

Acknowledgements

The authors wish to express their thanks to Assistant Professor I. UMEZAKI of the Koyto University for his useful suggestion on the sampling of seaweeds and seagrass and also for his kind identification of them.

References

BROOKS, R. R., J. LEE and T. JAFFRE (1974): Some New Zealand and New Caledonian plant accumulators of nickel. J. Ecology, **62**, 493-499.

BRYAN, G. W. (1973): The occurrence and seasonal variation of trace metals in the scallops *Pecten maximus* (L.) and *Chlamys opercularis* (L.). J. Mar. Biol. Ass. U. K., **53**, 145-166.

GILMAN, J. P. W. (1962): Metal carcinogenesis II. A study on the carcinogenic activity of cobalt, copper, iron, and nickel compounds. Cancer Res., **22**, 158-164.

HUTCHINSON, T. C. (1974): Heavy-metal pollution in the Sundbury mining and smelting region of Canada, I. Soil and vegetation contamination by nickel, copper, and other metals. Environmental Conservation, **1**, 123-132.

ICHIKAWA, R. (1961): On the concentration factors of some important radionuclides in the marine food organisms. Bull. Jap. Soc. Sci. Fish., **27**, 66-74.

KURATA, A. (1974): Cobalt content in the shallow sea sediments. J. Oceanogr. Soc. Jap., **30**, 199-202.

KURATA, A., Y. YOSHIDA, H. KADOTA and F. TAGUCHI (1977): Distribution of Ni-tolerant bacteria in water and sediments of the Sea of Aso. Bull. Jap. Soc. Sci. Fish., **43**, 1203-1208.

NISHIKAWA, K. and K. TABATA (1969): Studies on the toxicity of heavy metals to aquatic animals and the factors to decrease the toxicity—III. Bull. Tokai. Reg. Fish. Res. Lab., **58**, 233-241 (in Japanese).

PENTREATH, R. J. (1973): The accumulation from water of ^{65}Zn, ^{54}Mn, ^{58}Co and ^{50}Fe by the mussel, *Mytilus edulis*. J. Mar. Biol. Ass. U.K., **53**, 127-143.

PHILLIPS, D. J. H. (1976): The common mussel *Mytilus edulis* as an indicator of pollution by zinc, cadmium, lead and copper. I. Effect of environmental variables on uptake of metals. Mar. Biol., **38**, 59-69.

SUGIMURA, Y. (1972): Kaitei ni sonzai-suru busshitsu no kagaku. *In* MIYAKE, Y. (ed.): Kaiyo-kagaku kiso koza 12, Taiseki-butsu no kagaku. Tokai Univ. Press, Tokyo, p. 31-166.

阿蘇海におけるプランクトン，藻類および魚介類の Ni 蓄積

倉田　亮，吉田陽一，田口二三生

要旨: Ni 汚染の進行する阿蘇海の海水中および海底堆積物中の Ni 分布を調べ，合せてこの海域から採取したプランクトン，藻類，貝類および数種魚類などの Ni 蓄積について調べ，Ni 汚染の見られない海域のものと比較検討した。海底堆積物中の Ni 濃度は排出源から離れるほど低かった。この海域において採取したプランクトン，藻類および魚類などの組織中の Ni 濃度を Ni 汚染の見られない海域から採取したものと比べると，数倍～100 倍程度高く，また，他の金属類に比べて特に Ni 濃度のみ高く，これらの生物における著しい Ni 蓄積が認められた。海藻や水生植物ではスジアオノリ (*Enteromorpha prolifera*)，アマモ (*Zostera marina*) およびムカデノリ (*Grateloupia filicina*) の Ni 蓄積が著しく，貝類ではムラサキイガイ (*Mytilus edulis*) およびアサリ (*Tapes* (*Amygdala*) *japonica*) の，魚類ではボラ (*Mugil cephalus*) およびマハゼ (*Acanthogobius flavimanus*) などの Ni 蓄積が顕著であった。ボラでは特に鰓の Ni 蓄積が高かった。これら生物の Ni 濃縮係数は，最高 1,750 から数百の値を示し，概して藻類と貝類の Ni 濃縮が著しい傾向が見られたが，食物連鎖のレベルと Ni 濃縮係数との間には必ずしも明瞭な関係は見られなかった。

La mer (Bulletin de la Société franco-japonaise d'océanographie)
Tome 17, **N°** 1, **pp.** 18 à 27, Février 1979

Short Internal Waves on the Margin of the Continental Shelf of the East China Sea*

Akio MAEDA**

Abstract: Time series of temperature and current were taken during 3 days in the winter of 1975 on the margin of the continental shelf of the East China Sea. A current meter was moored at 82 m beneath the sea surface and another at 96 m. The vertical gradient of temperature is gentle at those depths, especially very small at 96 m. A five-cycle oscillation with a period of about 25 minutes is present in the temperature and velocity field. It is suggested, by the phase relation between the temperature and the current components as well as a theoretical analysis by the W.K.B. approximation applied to the vertical distribution of water density, that the 5-cycle oscillation should be the first mode internal waves propagating to the northeast parallel to the mean current and the Kuroshio in this region. The time series obtained by eliminating the tidal components M_2 and K_1 from the raw time series shows a random variation almost all over the measurement period except during the 5-cycle oscillation. A spectrum analysis was applied to the random variation. The random velocity field is anisotropic at both depths. The principal axis of the current ellipse of short period fluctuations of velocity is nearly parallel to the Kuroshio axis at 82 m and almost perpendicular to it at 96 m. The random current variation perpendicular to the Kuroshio axis plays an impartant role in processes of horizontal mixing of the shelf water with the Kuroshio water. The spectra of temperature and current at 82 m show significant peaks at a period of 27 minutes. It is also the case with the temperature spectrum at 96 m.

1. Introduction

The Kuroshio water changes its character in the course of the continental slope of the East China Sea (NITANI, 1972). The change is made by mixing of the shelf water with the Kuroshio water. However, our knowledge so far obtained is mainly based on the water mass analysis, and not on the direct current measurements. For the present, no material enough to deploy the current meter array for a very long period is available. Then, as a first step, an observation by moored current meters is made near the margin of the continental shelf for a short period, which allows us to have insight into the mechanism of the mixing resulting from the fluctuation short enough to be resolved.

Short period fluctuations of temperature have been studied by measurements in many regions, and are considered to be caused by turbulent motions (BYSHEVEND *et al.*, 1971) or by internal waves (HALPERN, 1971; MAEDA, 1974). Turbulent motions can carry mass, though internal waves can not. Because the mixing is associated with the mass transport, it is crucial to make clear whether the fluctuation is caused by turbulent motions or internal waves. Together with the current measurement, temperature measurements by thermometers incorporated in the current meter are planned in order to obtain phase relations between the temperature and current components, which should be useful for the present study if the coherences between them are high.

A distinct cyclic oscillation in a more or less random temperature record is observed, without current measurement, in the seasonal thermocline in several regions (ZIEGENBEIN, 1969, 1970; HALPERN, 1971; MAEDA, 1974). In this regard, too, the information on the current supplementing the information on the temperature should

* Recieved November 3, 1978
** Department of Marine Civil Engineering, Faculty of Engineering, Kagoshima University, 1-21-40 Koorimoto, Kagoshima, 890 Japan

be useful: if such an oscillation is due to internal waves, those informations should indicate the direction of the wave propagation.

Previous data suggest that the isotherms and isohalines run nearly parallel to the mean axis of the Kuroshio at the moored station. So, the fluctuation component perpendicular to the Kuroshio axis is more effective in the transport of heat and salinity than that parallel to it. This can be studied by phase relations between the current components and the temperature.

2. Observation and description of its results

Two current meters were moored at 82 m and 96 m below the sea surface at Sta. A (27°40′N, 125°30′E) 110 m deep (Fig. 1). Station A is some 270 km distant from Okinawa to the northwest. The measurement was made every 5 minutes during about 3 days from 19th to 22nd February 1975. In parallel with the measurement, STD cast was made at intervals of 3 hours on board of the R.V. Hakuhomaru (Ocean Research Institute, University of Tokyo) during 2 days from 19th to 20th February till the cast was ceased because of a stormy wind.

A temperature section of the Kuroshio was observed by XBT nearly along the line from Sta. 1 (28°N, 125°E) to Sta. 23 (26°44′N, 126°42′E) till 23rd February after the recovery of the current meters. The stations were occupied at intervals of 5 miles. When the vessel was returning to Sta. 1, STD and XBT casts were alternately made at approximately the same stations as before.

The axis of Kuroshio is situated near Sta. 17 at 20 miles distant from the margin of the continental shelf (Figs. 2 and 3). Station A is

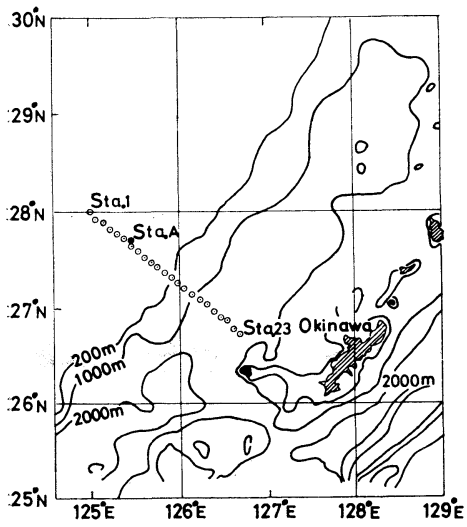

Fig. 1. Stations of observation. STD and XBT casts were made at Stas. 1 (28°N, 125°E) through 23 (26°44′N, 126°42′E) which are shown by symbols ⊙. Current measurements were made at Sta. A (27°40′N, 125°30′E).

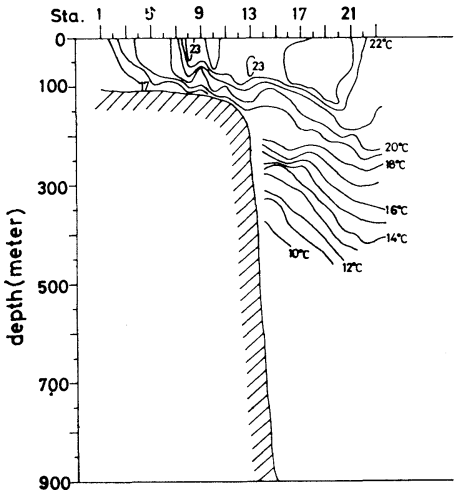

Fig. 2. Temperature section of the Kuroshio. A thermal front exists between Stas. 7 and 8.

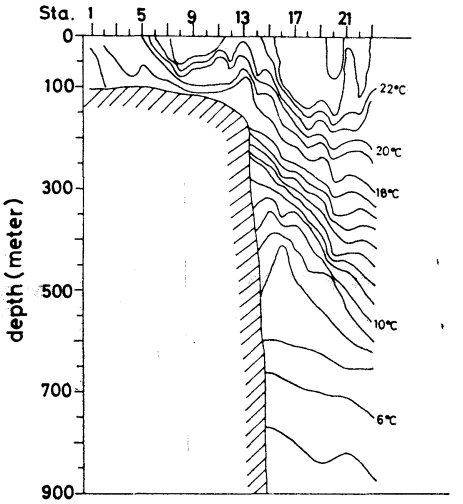

Fig. 3. Temperature section of the Kuroshio (returning). The thermal front shifts to an area between Stas. 6 and 7.

53 miles distant from Sta. 17 by a thermal front. The current meter is in the lower part of the thermocline (Fig. 4). The mean vertical gradient of temperature is about 1.5×10^{-2}°C/m at 82 m and 0.9×10^{-2}°C/m at 96 m, respectively. The mean Väisälä frequency is about 3.36×10^{-1} min^{-1} and 1.97×10^{-1} min^{-1} at those depths, respectively.

Semi-diurnal and diurnal components predominate in the current fluctuations measured at 82 m and 96 m, but not in temperature fluctuations. The magnitude and direction of the predominant components are estimated by the method of least squares on the assumption that those periods were of M_2 and K_1 tide. The results are shown in Table 1. The direction is clockwisely counted from the north. The both tidal components elliptically rotate in clockwise direction at both depths. We shall discuss no more about the tide, because our interest is in shorter period fluctuations, and in addition to it, the measurement period is too short to study the tides. The time series obtained by filtering out the components of

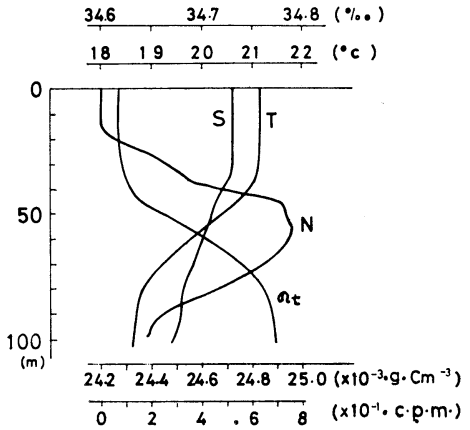

Fig. 4. Mean vertical distributions influencing short period fluctuations. T is temperature, S salinity, N Väisälä frequency and σ_t density.

Table 1. Tidal currents and mean currents.

Depth	Comp.	Max. vel.	Main direct.	Ratio of axes	Mean currents	
					absolute	direct.
82 m	M_2	7.9 cm/s	247°	0.38	19.6 cm/s	67°
	K_1	4.5 cm/s	139°	0.27		
96 m	M_2	12.2 cm/s	237°	0.48	8.2 cm/s	50°
	K_1	8.6 cm/s	180°	0.44		

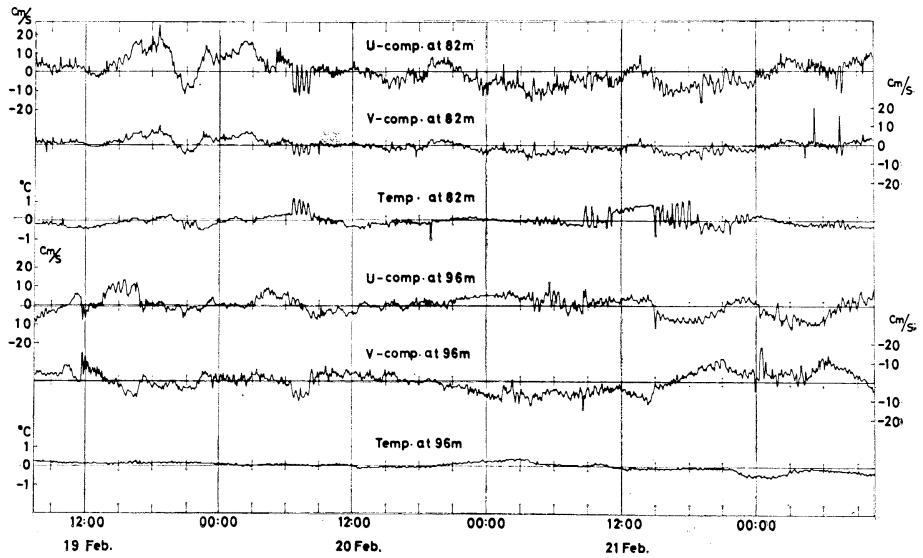

Fig. 5. The filtered fluctuations of current and temperature at 82 m and 96 m.

tidal periods are shown in Fig. 5.

The current and temperature oscillate with a period about 25 minutes (0.251 c.p.m.) at 82 m from 6:00 to 8:00 on 20th February, though they irregularly fluctuate at other times (Fig. 5). The amplitude of the eastward component u is about 6 cm/s and that of the northward component v is about 3 cm/s. Because the both components are in phase, the azimuth α of horizontal oscillations can be easily calculated from $\alpha=\tan^{-1}u/v\fallingdotseq\tan^{-1}2$, where α is clockwisely counted from the north. The result, $\alpha\fallingdotseq63°$, indicates nearly the direction of the average current (Table 1). We can suppose that these periodic oscillations may be due to internal waves. So, it will be valuable to make theoretical considerations about the mechanisms of internal waves.

3. Theoretical consideration on the periodic oscillations

Taking the horizontal axis x positive toward the direction of propagation of internal waves and the vertical axis z positive downward, we have the vertical velocity w by internal waves

$$w=a(z)\cdot\cos(k\cdot x-\omega\cdot t)\,, \qquad (1)$$

where $a(z)$ is the amplitude at z below the sea surface, k the wave number, ω the angular frequency and t the time. On substituting (1) for the two dimensional equation of continuity for an incompressible fluid, the horizontal velocity v becomes

$$v=-\frac{1}{k}\cdot\frac{da}{dz}\cdot\sin(k\cdot x-\omega\cdot t). \qquad (2)$$

The integral constant is disregarded because it is not important to our discussion. Because the vertical gradient of temperature is very large compared with the horizontal one, the conservation equation of temperature will be approximated by

$$\frac{\partial\theta}{\partial t}+\left\langle\frac{\partial\theta}{\partial z}\right\rangle\cdot w=0\,, \qquad (3)$$

by ignoring the mixing of heat, where θ is the temperature and $\langle\partial\theta/\partial z\rangle$ is the time mean of the vertical gradient of temperature. Substituting (1) for (3) and integrating with respect to time, we have

$$\theta=\frac{1}{\omega}\cdot\left\langle\frac{\partial\theta}{\partial z}\right\rangle\cdot a\cdot\sin(k\cdot x-\omega\cdot t)\,, \qquad (4)$$

where the integral constant is also disregarded. The oscillations of current are out of phase with those of temperature at 82 m. Accordingly, the relation of amplitude between the temperature and the current must be

$$\left(-\frac{1}{k}\cdot\frac{da}{dz}\right)\cdot\left(\frac{1}{\omega}\left\langle\frac{\partial\theta}{\partial z}\right\rangle\cdot a\right)<0\,. \qquad (5)$$

Because $k>0$, $\omega>0$, and $\langle\partial\theta/\partial z\rangle<0$, we have

$$\frac{da}{dz}\cdot a<0 \text{ so that } \frac{da^2}{dz}<0\,. \qquad (6)$$

Relations (6) show that the absolute value of amplitude of vertical velocity increases upward at 82 m.

The vertical distribution of amplitude depends on the mode of internal waves. The vertical distribution of relative amplitude can be approximated from the vertical distribution of density (ECKART, 1960). The approximation gives the wave number corresponding to each mode. This is very accurate for higher modes, but not so for lower ones. Then, the lower modes determined by this method must be tested by some other methods.

If we put $a(z)=A\cdot\sin S(z)$, the W.K.B. approximation gives the following relation between the Väisälä frequency $N(z)$, the frequency of internal waves ω and the wave number,

$$S(z_2)-S(z_1)=\frac{k_m}{\omega}\int_{z_1}^{z_2}(N^2(z)-\omega^2)^{1/2}dz =(m+\Delta)\pi\,, \qquad (7)$$

where m is the mode number, k_m the wave number of mode m and Δ the error resulting from the various approximations involved in (7). The mode number m gives the number of the maximums of wave amplitudes in the layer between z_1 and z_2 which are selected as follows,

$$N(z_1)=N(z_2)=\omega \text{ and } \omega<N(z) \text{ for } z_1<z<z_2\,.$$

The error Δ is small for large m. The numerical

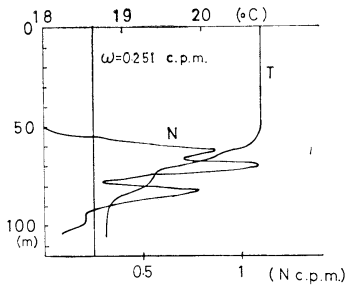

Fig. 6. Vertical distributions of temperature and Väisälä frequency during the periodic oscillations. The temperature and the Väisälä frequency are averaged over 6:00 to 9:00 on 20th.

Table 2. Wave numbers k_m, lengths L_m and phase velocities c_m calculated by the W.K.B.

Mode No.	k_m ($\times 10^{-4}$ cm^{-1})	L_m ($\times 10^4$ cm)	c_m (cm/sec)
1	3.83	1.64	10.94
2	7.66	0.82	5.47
3	11.49	0.55	3.65
4	15.32	0.41	2.73
5	19.15	0.32	2.19

integration of (7) gives the wave number k_m, that is, the wave length L_m, and the relative vertical distribution of the amplitude of w for each mode. The lower limit z_1 of integration is chosen to be 55 m and the upper limit z_2 92 m, both determined from the averaged distribution $N(z)$ during the oscillations and the angular frequency $\omega=0.251$ c.p.m. (Fig. 6). The numerical integration was made for the first mode to the fifth. The result is given in Table 2. According to equation (2), the term $1/k_m \cdot da_m/dz$ at 82 m can be estimated from the amplitude of horizontal velocity. Because the amplitude of horizontal velocity is 6.71 cm/s in our measurement, we have

$$\frac{1}{k_m} \cdot \frac{da_m}{dz}\Bigg|_{z=82\,\mathrm{m}} = 6.71\,(\mathrm{cm/s}). \quad (8)$$

On the other hand, the quantity $1/k_m \cdot da_m/dz$ at 82 m can be also determined from the vertical gradient of the amplitude of internal waves together with the wave numbers k_m shown in Table 2. Because the W.K.B. approximation gives the relative vertical distribution

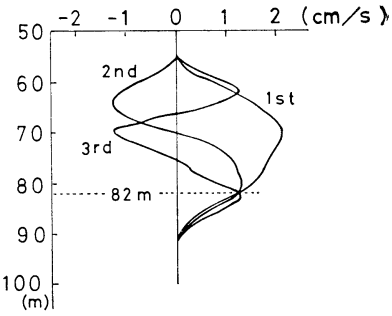

Fig. 7. Vertical distributions of amplitude of vertical velocity calculated for the first three modes. The amplitudes are given 1.2 cm/s at 82 m which is obtained from the vertical gradient of temperature and from the amplitude of temperature fluctuations.

Table 3. Amplitudes of horizontal velocity calculated from the observed amplitude of temperature and from the wave numbers shown in Table 2.

Mode No.	1	2	3
$1/k_m \cdot da_m/dz$ (cm)	5.91	1.75	0.99

of the amplitude of vertical velocity for each mode, the absolute amplitude of vertical velocity at an arbitrary depth is determined from that at 82 m. By using Eq. (3), the amplitude of vertical velocity at 82 m can be obtained from the temperature amplitude 0.2°C at 82 m and the vertical gradient of temperature 0.07°C/m at 82 m. Figure 7 shows the resulting vertical distribution of the amplitude of vertical velocity for the first three modes. The term $1/k_m \cdot da_m/dz$ is calculated for the first three modes and shown in Table 3. Table 3 shows that the calculated amplitude for the first mode takes the value nearest to the measurement one (Eq. (8)). Moreover, Fig. 7 shows that the first mode also satisfies the relation (6). Consequently, the repeating oscillations are interpreted as first mode internal waves.

4. Spectrum analysis

The B-T analysis is applied to the time series obtained eliminating the tidal components. Figures 8-a and 8-b show the spectra of the temperature and the two components of the current velocity at 82 m and 96 m. These spectra are estimated with 18 degrees of freedom.

The spectra of temperature and current at 82 m show significantly higher energy level in the range between the 12th frequency (0.024 c.p.m.) and the 22nd (0.038 c.p.m.) than in the other frequency range. Precisely, the peak is found at the 18th frequency (0.036 c.p.m.) for the temperature and at the 19th (0.038 c.p.m.) for the current which are equivalent to the period of 26.3 minutes and 27.8, respectively. The peak may be subject to some effect of the periodic oscillations mentioned above. However, though such periodic oscillations are not detected at 96 m, the temperature spectrum at 96 m has

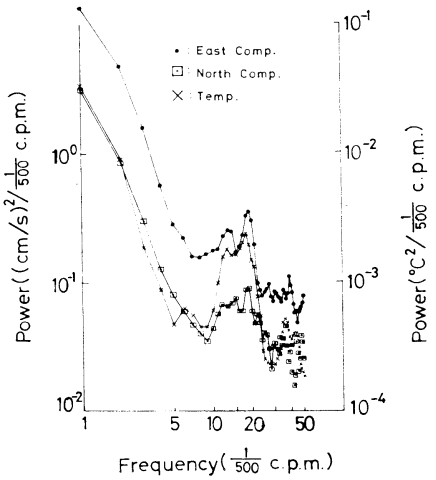

Fig. 8-a. Spectra of temperature and current fluctuations at 82 m.

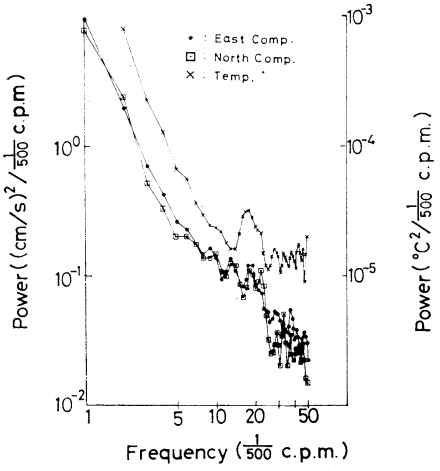

Fig. 8-b. Spectra of temperature and current fluctuations at 96 m.

also a significant peak at the 18th frequency. The current spectra at 96 m have a peak, though not very significant at the 18th frequency.

Figures 9-a through 9-c show the coherences between the temperatures and the current components at the two depths, and Figs. 10-a through 10-c show the phase differences. The coherence between the eastward and the northward components at 82 m is far over the level which gives the limit of the probability of 0-correlation in 95% confidence (Fig. 9-a). According to the very high level of the coherence, the phase difference between the two components is reliable and nearly 0 degree (Fig. 10-a). The energy level of the eastward component is nearly equal to that of the northward component at 82 m (Fig. 8-a). The equalities of the phase and of the energy density show that the horizontal velocity varies approximately along the line running from the southwest to the northeast, parallel to the average current (Table 1).

The phase difference between the two components at 96 m is also reliable because of the coherence between them higher than the 0-level (Fig. 9-a). The phase difference is about 180 degrees (Fig. 10-a). According to the phase difference and the equality in the energy levels of the two components at 96 m (Fig. 8-b), the horizontal current at 96 m varies mainly along the line running from the southeast to the northwest, perpendicular to the variation line at 82 m. These features suggest the complexity of the current field near the front.

The vertical structure of the current field should be estimated from the phase relations between the currents at different depths, if the coherence between them is higher than the 0-correlation level. The coherence between the eastward component at 82 m and the northward component at 96 m is over the level in the frequency range from the 15th (0.03 c.p.m.) to 20th (0.04 c.p.m.) (Fig. 10-b). The phase difference in this frequency range is reliable. This is only 0 to 10 degrees in this range (Fig. 10-b). The difference between the northward component at 96 m is 160 to 180 degrees in the same frequency range in which the coherence between them is slightly over the 0-level. If

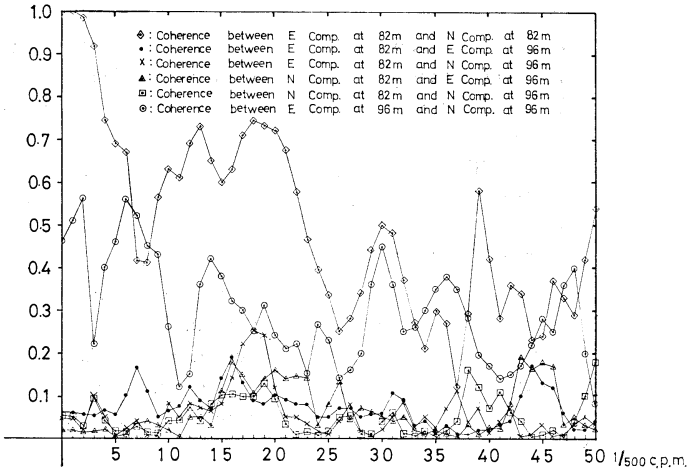

Fig. 9-a. Coherences between current components.

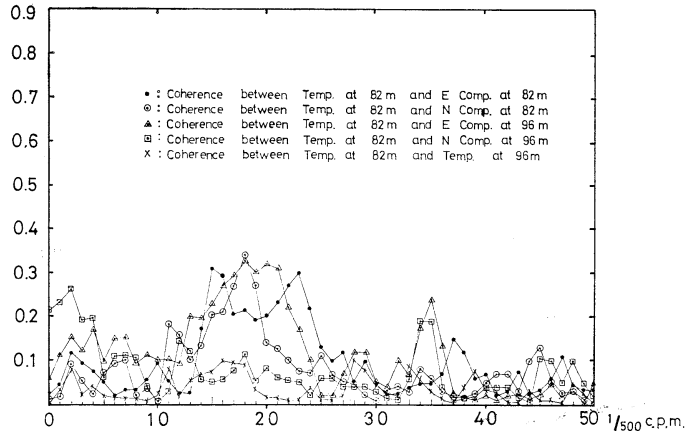

Fig. 9-b. Coherences between temperature at 82 m and others.

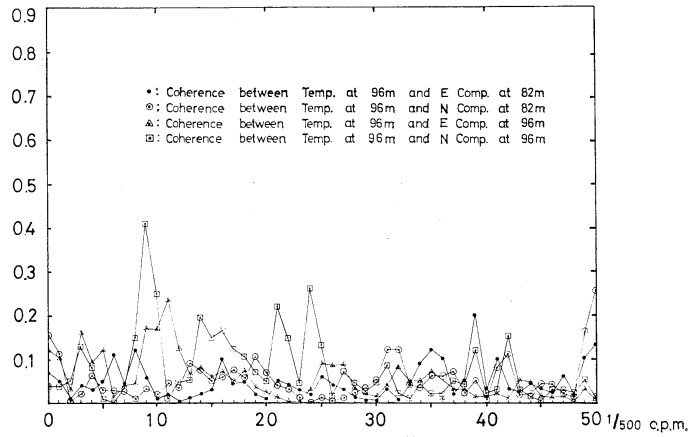

Fig. 9-c. Coherences between temperature at 96 m and others.

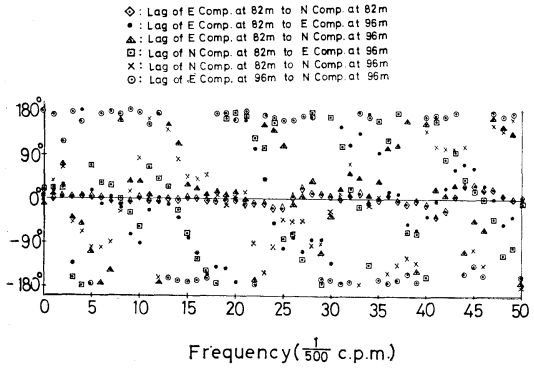

Fig. 10-a. Phase differences between current components.

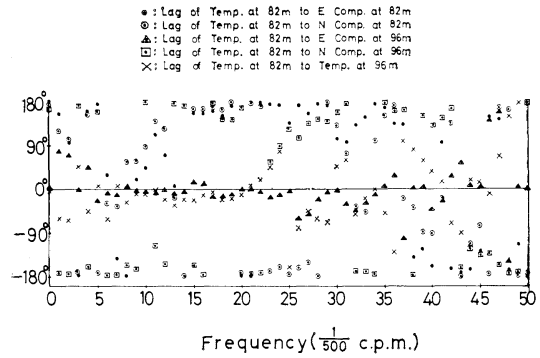

Fig. 10-b. Phase differences between temperature at 82 m and others.

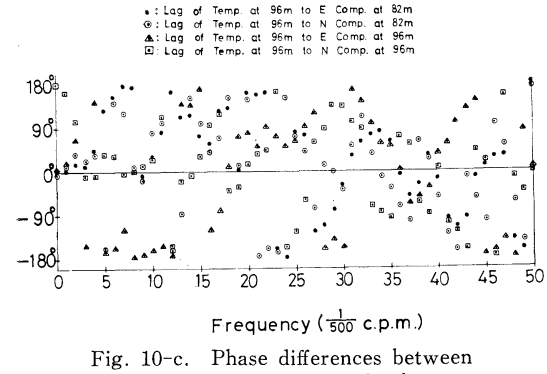

Fig. 10-c. Phase differences between temperature at 96 m and others.

the phase difference is reliable, the fluctuations in this range at 82 m flow to the northeast, while those at 96 m flow to the northwest, that is to say, the axis of current fluctuations counterclockwisely rotates with increasing depth.

The coherences between the temperature and the two current components at 82 m are over the level in the frequency range from the 12th to 22nd where the temperature and the two components take higher energy densities than those on either side of the range (Fig. 8-a and Fig. 9-b). The phase of temperature differs by 160 to 180 degrees from the phases of the two components (Fig. 10-c). This means that the current flows to the southwest at 82 m when the temperature rises. If the higher energy densities of temperature and of the two components at 82 m are caused by internal waves of the first mode with the frequency range from the 12th to 22nd, the phase relations indicate that the internal waves will propagate to the northeast.

The phase difference between the temperature and the northward component at 92 m is reliable in the frequency range from the 8th (0.016 c.p.m.) to the 10th (0.020 c.p.m.), and takes 0 to 20 degrees (Figs. 9-c and 10-c). The phase difference between the temperature and the eastward component at 96 m is also reliable in the range from the 9th (0.018 c.p.m.) to the 11th (0.022 c.p.m.) and takes 160 to 180 degrees. Consequently, the temperature rises when the current flows to the northwest. If the temperature and current fluctuations in this range at 96 m should be due to vertical displacements of the sea water by internal waves, those at 82 m will show higher coherence between the temperature at 82 m and the current velocity at 96 m because the vertical gradient of temperature is sharper at 82 m than at 96 m. The station of the current measurement is only 5 miles distant from the thermal front to the northwest (Figs. 2 and 3). The front reaches down to the bottom and may be nearly parallel to the Kuroshio axis. Therefore, the fluctuations of the horizontal current are able to produce a considerable part of the temperature fluctuations. Because the temperature near the station increases toward the southeast, the temperature at the station will rise when the current flows to the northwest and vice versa. Actually, the observed phase relation coincides with this tendency. If the fluctuations are mainly due to turbulent motions, they will play an effective role in the transport of heat and salt.

5. Discussion

The present observation does not make thoroughly clear the mechanism of internal waves of short periods, because the measurements of temperature and of current are made unexpectedly at the lower part, not in the central part, of the thermocline which was unusually shallower in that time than the thermocline estimated from previous data. The tidal period M_2 and K_1 predominate in the fluctuations of current at the both depths. The tidal current may be due to the surface mode, because the tidal period does not appear in temperature fluctuations.

Though the temperature and filtered current records randomly vary in almost all over the measurement period, the periodic oscillation continues for about 2 hours with a period of 25 minutes. According to the phase relation between the temperature and the current and by the application of the W.K.B. approximation, the periodic oscillations are probably due to the first mode internal waves. The first mode waves may be propagating to the northeast, that is the mean current direction, although the determination of their propagation direction lacks an accuracy because of the uncertainty of the determination of mode.

As mentioned above, the present study is a preliminary step. There should be some difficulties in carrying out a more substantial study as a next step. The precise determination of the direction of the wave propagation requires a finer vertical spacing of the temperature and current measurements. The direction can be also determined by temperature time series obtained at three points located on a horizontal plane in the thermocline, whose accuracy mainly depends on how accurately one can keep the horizontal distance between the stations which should be short enough compared with the wave length to be dealt with. Because the wave length is generally short (Table 2), its maintenance is difficult in deep open ocean. We shall overcome these difficulties in the near future.

The coherence between the temperature and the current is higher than the level of the 0-correlation in the range from 0.03 c.p.m. to 0.04 where the spectra of temperature at the both depths and of current at 82 m rise. The spectrum rise is thought due to internal waves propagating to the northeast. In this case, the precise determination of their mode is also important to the precise determination of their direction.

The current fluctuations at 82 m predominate in the direction parallel to the mean current in all the frequency range considered. On the contrary, the fluctuations at 96 m predominate in the direction perpendicular to it. The prependicular fluctuations are thought to play an important role in mixing of the Kuroshio water and the shelf water in this season. It is necessary to ascertain whether the fluctuations perpendicular to the passage of the Kuroshio are present irrespective of the time or not.

Acknowledgements

The observation was carried out in KH-75-2 Cruise of the Hakuhomaru, the Ocean Research Institute. The author is much indebted to her crew for the mooring of current meters and for the hydrographic casts. He wishes to express his thanks to Prof. M. TOMINAGA of Kagoshima University for the helpful discussion and to Mr. F. IKEDA for his help in drafting.

References

BYSHEVEND, V.I., YU. A. IVANOV and YE. G. MOROGOV (1971): Study of temperature fluctuations in the frequency range of internal gravity waves. Atmospheric and Oceanic Physics, **7**, 25-30.

ECKART, C. (1960): Hydrodynamics of Oceans and Atmospheres. Pergamon Press, New York, 290 pp.

HALPERN, D. (1971): Observations on short-period internal waves in Massachusetts Bay. J. Marine Res., **29**, 116-131.

MAEDA, A. (1974): A description of short period temperature fluctuations in the upper ocean. J. Oceanogr. Soc. Japan, **30**, 121-136.

NITANI, H. (1972): Beginning of the Kuroshio, Chapter 5 in Kuroshio edited by H. STOMMEL and K. YOSHIDA. Univ. of Tokyo Press, 517 pp.

ZIEGENBEIN, J. (1969): Short internal waves in the Strait of Gibraltar. Deep Sea Res., **16**, 479-487.

ZIEGENBEIN, J. (1970): Spatial observations of short period internal waves in the Strait of Gibraltar. Deep Sea Res., **17**, 867-875.

東シナ海大陸棚縁での短周期内部波の観測

前　田　明　夫

要旨: 1975年2月19日から2月22日の3日間，東シナ海大陸棚の縁近くの点（北緯27度40分，東経130度30分，水深 110 m）に流速計2台を係留し，水温及び流速の時間シリーズの測定をした。測定層は 82 m 深と 96 m 深である。この測流に平行して3時間に1回の STD 観測をおこなった。測流層における水温の鉛直勾配は小さく，特に 96 m 深では著しく，そのため水温変動の振幅が小さかった。周期約 25 分の顕著な水温及び流速の振動が5波続くのが発見された。水温と流速の位相関係及び W.K.B. 近似によると，この振動は北東に伝搬する第1モードの内部波であることが推定された。この伝搬方向はほぼ平均流と同じであり，この海域の黒潮の方向にほぼ一致している。流速は半日周期と1日周期が卓越していたが，これらを潮汐成分 M_2 K_1 であるとして消去したものは，先の周期的振動の期間以外では，ほぼランダムに変動していた。スペクトル解析によると，82 m 深の流速変動及び 82 m 深と 96 m 深における水温変動では約 27 分の周期が卓越していることがわかった。関連度関数及び位相差から，対象とする周波数全域で 82 m 深では北東～南西の振動が卓越し，わずか 14 m 下層の 96 m 深ではこれとほぼ直交する北西～南東の振動が卓越していることがわかった。

La mer (Bulletin de la Société franco-japonaise d'océanographie)
Tome 17, N° 1, pp. 28 à 32, Février 1979

円弧状海岸の線型波について*

中　村　重　久**

Sur l'Ondulation Linéaire le long de la Côte Circulaire

Shigehisa NAKAMURA

Résumé: Pour rechercher sur l'ondulation progressive qui se propage le long de la côte circulaire, on transforme les équations fondamentales ecrites en coordonnées cylindriques en une paire de deux équations différentielles. La solution donne les profils de l'ondulation au large de la côte circulaire. L'auteur a donneé par ailleurs une remarque dans le cas où l'effet de la rotation de la terre est négligeable comme dans le cas de l'expérience hydraulique.

1. 緒　言

わが国で太平洋に面している海浜をみると，一般に彎曲している。海に向って凸な海浜もまれにみられるが，凹な海浜が多い。これまでに，半無限海に面した直線状海岸におけるエッジ波の研究(中村，1976a, b)[1)2)]があるけれども，海岸線の彎曲の効果の検討には，別の面からの解折をすすめる必要がある。ここでは，円柱座標系における基礎方程式から漸近的線型微分方程式を導き，円弧状海岸における線型波の波高分布を理論的にもとめ，海岸線の彎曲の効果，海底こう配の効果，地球自転の効果について検討する。さらに，地球自転の効果が無視できるような場合についても考察をすすめ，水槽実験における問題点についても説明を加える。

2. 基礎方程式

円弧状の海岸線が無限に広い海に面している場合を考える。平均海面を $r\theta$ 平面とし，z 軸を鉛直上向にとり，円弧の曲率の中心を原点とする円柱座標を考える。擾乱による海面の変位は水深に比べて微小であり，ζ であらわされるものとする。このとき，基礎方程式

$$\left.\begin{aligned}&\frac{\partial u}{\partial t}+g\frac{\partial \zeta}{\partial r}-fv=\frac{\partial P_a}{\partial r},\\&\frac{\partial v}{\partial t}+g\frac{1}{r}\frac{\partial \zeta}{\partial \theta}+fu=\frac{1}{r}\frac{\partial P_a}{\partial \theta},\\&\frac{\partial \zeta}{\partial t}=-\int_{-h}^{\zeta}\left[\frac{\partial u}{\partial r}+\frac{1}{r}\frac{\partial v}{\partial \theta}\right]dz\end{aligned}\right\}\qquad(1)$$

を出発点とする。ここに，u および v は流速の r および θ 方向成分，h は水深，g は重力加速度，f はコリオリの効果に関するもので $f=2\Omega\sin\varphi$，そして，φ は着目する水域の緯度である。ただし，ここでは，重力以外の外力の作用の効果を P_a で表すことにした。

解析を簡単にする便宜的手法として，

$$\int_{-h}^{\zeta}u\,dz=U,\quad\int_{-h}^{\zeta}v\,dz=V\qquad(2)$$

と書くことにし，さらに，

$$\int_{-h}^{\zeta}\frac{\partial P_a}{\partial r}dz=\frac{\partial F}{\partial r},\quad\int_{-h}^{\zeta}\frac{\partial P_a}{\partial \theta}dz=\frac{\partial F}{\partial \theta}\qquad(3)$$

と書ける場合には，(2) および (3) を用いて，(1) はつぎのように書きかえられる。すなわち，

* 1978年11月 1 日受理
** 京都大学防災研究所，宇治市五ケ庄
Disaster Prevention Research Institute, Kyoto University, Uji, Kyoto, 611 Japan

$$\left.\begin{aligned}&\frac{\partial U}{\partial t}+gh\frac{\partial \zeta}{\partial r}-fV=\frac{\partial F}{\partial r},\\&\frac{\partial V}{\partial t}+gh\frac{1}{r}\frac{\partial \zeta}{\partial \theta}-fU=\frac{1}{r}\frac{\partial F}{\partial \theta},\\&\frac{\partial \zeta}{\partial t}=\frac{\partial U}{\partial r}+\frac{1}{r}\frac{\partial V}{\partial \theta}.\end{aligned}\right\}\quad(4)$$

さらに，(4) の未知関数 U, V, ζ および F が，

$$\left.\begin{aligned}&U=u_0\exp(i\omega t),\\&V=v_0\exp(i\omega t),\\&\zeta=z_0\exp(i\omega t),\\&F=F_0\exp(i\omega t)\end{aligned}\right\}\quad(5)$$

と書けるとすると，(5) を (4) に代入した後，それぞれのサフィクスをとり去ることにより，

$$\left.\begin{aligned}&i\omega u+gh\frac{\partial z}{\partial r}-fv=\frac{\partial F}{\partial r},\\&i\omega v+gh\frac{1}{r}\frac{\partial z}{\partial \theta}+fu=\frac{1}{r}\frac{\partial F}{\partial \theta},\\&i\omega z=\frac{\partial u}{\partial r}+\frac{1}{r}\frac{\partial v}{\partial \theta}.\end{aligned}\right\}\quad(6)$$

とくに，$F=0$ の場合には，

$$\left.\begin{aligned}&i\omega u+gh\frac{\partial z}{\partial r}-fv=0,\\&i\omega v+gh\frac{1}{r}\frac{\partial z}{\partial \theta}+fu=0,\\&i\omega z=\frac{\partial u}{\partial r}+\frac{1}{r}\frac{\partial v}{\partial \theta}.\end{aligned}\right\}\quad(7)$$

3. 凹海岸における波

海岸線が凸な場合で，海岸線 $r=r_0$ からの距離に比例して水深が変化する場合を考える。このとき，

$$h=\alpha(r_0-r),\quad r\leqq r_0.\qquad(8)$$

ただし，α は正の実数である。

この場合，前節に導いた基礎方程式 (7) は，

$$\left.\begin{aligned}&i\omega u+g\alpha(r_0-r)\frac{\partial z}{\partial r}-fv=0,\\&i\omega v+g\alpha(r_0-r)\frac{1}{r}\frac{\partial z}{\partial \theta}+fu=0,\\&i\omega z=\frac{\partial u}{\partial r}+\frac{1}{r}\frac{\partial v}{\partial \theta}.\end{aligned}\right\}\quad(9)$$

(9) の第1式に f を，第2式に $i\omega$ をそれぞれ乗じ，v をもとめると

$$v=\frac{-g\alpha(r_0-r)}{f^2-\omega^2}\left(f\frac{\partial z}{\partial r}-\frac{i\omega}{r}\frac{\partial z}{\partial \theta}\right).\qquad(10)$$

同様に，(9) の第1式に $i\omega$ を，第2式に f をそれぞれ乗じ，u をもとめると

$$u=\frac{-g\alpha(r_0-r)}{f^2-\omega^2}\left(i\omega\frac{\partial z}{\partial r}-\frac{f}{r}\frac{\partial z}{\partial \theta}\right).\qquad(11)$$

さらに，(10) および (11) を (9) の第3式に代入すると

$$\begin{aligned}(f^2-\omega^2)i\omega z=&-g\alpha(r_0-r)\\&\times\left[i\omega\frac{\partial^2 z}{\partial p^2}+\frac{f}{r^2}\frac{\partial z}{\partial \theta}-\frac{i\omega}{r^2}\frac{\partial^2 z}{\partial \theta^2}\right]\\&+g\alpha\left[i\omega\frac{\partial z}{\partial r}-\frac{f}{r}\frac{\partial z}{\partial \theta}\right].\end{aligned}\qquad(12)$$

ここで，z の解が変数 r および θ に対して変数分離形

$$z=R(r)\,\Theta(\theta)\qquad(13)$$

で与えられるものとする。このとき，(13) と (12) とから，任意の複素数 k に対して，

$$\left.\begin{aligned}&i\omega\frac{r^2}{R}\frac{d^2R}{dr^2}+\frac{i\omega}{r_0-r}\frac{r^2}{R}\frac{dR}{dr}+\frac{\alpha_0 r^2}{r_0-r}=ik,\\&\frac{i\omega}{\Theta}\frac{d^2\Theta}{d\theta^2}+\left(\frac{r}{r_0-r}-1\right)\frac{f}{\Theta}\frac{d\Theta}{d\theta}=ik.\end{aligned}\right\}\quad(14)$$

ただし，

$$\alpha_0=\frac{(f^2-\omega^2)i\omega}{g\alpha}.\qquad(15)$$

一般に (14) はかならずしも簡単な解をもたないようである。(14) の式の特長をとらえるために，ここでは，つぎのような極端な2例を考える。すなわち，(A) r_0 が十分大きい場合 ($r_0\to\infty$) と (B) r_0 が十分小さい場合 ($r_0\ll r$) とである。ここで，解析解がもとまったとしても，物理的に意味のないものが得られる場合もありうるので注意をしなくてはならない。

(A) r_0 が十分大きい場合，海岸線のごく近くの

水域に着目することにすると，(14) の第2式で

$$\left(\frac{r}{r_0-r}-1\right)\to -1 \qquad (16)$$

となる。ここで，便宜的に

$$s=r_0-r \qquad (17)$$

を用いることにすると，(41) は

$$\left.\begin{aligned}&\frac{d^2R}{ds^2}-\frac{1}{s}\frac{dR}{ds}+\left(\frac{\alpha_0}{s}-\frac{ik}{(r_0-s)^2}\right)\frac{R}{i\omega}\\&\qquad=0,\\&\frac{d^2\Theta}{d\theta^2}-\frac{f}{i\omega}\frac{d\Theta}{d\theta}-\frac{k}{\omega}\Theta=0.\end{aligned}\right\} \qquad (18)$$

そして，r が十分大きな場合には，k を含む項は (18) 第1式では無視できるものと考えられ，漸近的に[3]

$$\frac{d^2R}{ds^2}-\frac{1}{s}\frac{dR}{ds}+\frac{\alpha_0}{i\omega s}R=0 \qquad (19)$$

と書ける。さらに，(15) を考慮すると，

$$\frac{d^2R}{ds^2}-\frac{1}{s}\frac{dR}{ds}+\frac{f^2-\omega^2}{g\alpha}\frac{1}{s}R=0. \qquad (20)$$

(20) の一般解は

$$R=R_0\cdot(r_0-r)\times Z_0\left(\pm 2\sqrt{\frac{f^2-w^2}{g\alpha}(r_0-r)},C\right) \qquad (21)$$

で与えられる。ただし，R_0 は定数，そして，

$$\left.\begin{aligned}&Z_\nu(z,0)=J_\nu(z),\\&Z_\nu(z,i)=H_\nu^{(1)}(z),\\&Z_\nu(z,\infty)=N_\nu(z),\\&Z_\nu(z,-i)=H_\nu^{(2)}(z),\end{aligned}\right\} \qquad (22)$$

であり，(22) はそれぞれ，ベッセル関数，第1種ハンケル関数，ノイマン関数，第2種ハンケル関数である。

(18) の第2式の解は簡単にもとまって，

$$\Theta=\Theta_1\exp(i\kappa_1\theta)+\Theta_2\exp(i\kappa_2\theta). \qquad (23)$$

ただし，κ_1 および κ_2 は次式を満足する。

$$\kappa^2-\frac{f}{\omega}\kappa+\frac{k}{\omega}=0. \qquad (24)$$

したがって，(21) と (23) とから，とくに $C=0$ の場合の解は

$$\zeta=R_0\cdot(r_0-r)\cdot J_0\left(2\sqrt{\frac{f^2-\omega^2}{g\alpha}(r_0-r)}\right)\times[\Theta_1\exp(i\kappa_1\theta)+\Theta_2\exp(i\kappa_2\theta)]\times\exp(i\omega t). \qquad (25)$$

ω が f より小さいときは，上式のように解はベッセル関数 $J_0(z)$ によって与えられるが，ω が f より大きい場合には，変形ベッセル関数 $I_0(z)$ を用いる必要がある。

(B) r_0 が十分小さく，着目する水域は海岸線から十分遠いとみなせる場合には，(14) の第2式で

$$\left(\frac{r}{r_0-r}-1\right)\to -2 \qquad (26)$$

であるから，(18) に対応する式は

$$\left.\begin{aligned}&\frac{d^2R}{ds^2}-\frac{1}{s}\frac{dR}{ds}+\left(\frac{\alpha_0}{s}-\frac{ik}{(r_0-s)^2}\right)\frac{R}{i\omega}\\&\qquad=0,\\&\frac{d^2\Theta}{d\theta^2}-\frac{2f}{i\omega}\frac{d\Theta}{d\theta}-\frac{k}{\omega}\Theta=0\end{aligned}\right\} \qquad (27)$$

ここで，r_0 が十分小さいことを考慮すると，(27) 第1式は漸近的に

$$\frac{d^2R}{ds^2}-\frac{1}{s}\frac{dR}{ds}+\frac{\alpha_0 s-ik}{i\omega s^2}R=0 \qquad (28)$$

あるいは，さらに書きかえて，

$$\frac{d^2R}{ds^2}-\frac{1}{s}\frac{dR}{ds}+\left[\frac{(f^2-\omega^2)}{g\alpha}\frac{1}{s}-\frac{k}{\omega s^2}\right]R=0 \qquad (29)$$

この式の解は

$$R=R'_0\cdot(r_0-r)\times Z_{4(1-k/\omega)}\left(\pm 2\sqrt{\frac{f^2-\omega^2}{g\alpha}(r_0-r)},C\right). \qquad (30)$$

また，(27) 第2式の解は (23) と同型であるが，κ_1 および κ_2 は

$$\kappa^2-\frac{2f}{\omega}\kappa+\frac{k}{\omega}=0 \qquad (31)$$

を満す。したがって，とくに $C=0$ の場合の解は

$$\zeta=R_0'\cdot(r_0-r)\cdot\left[J_{4(1-k/\omega)}\left(2\sqrt{\frac{f^2-\omega^2}{g\alpha}(r_0-r)}\right)\right.$$
$$\left.-J_{-4(1-k/\omega)}\left(2\sqrt{\frac{f^2-\omega^2}{g\alpha}(r_0-r)}\right)\right]$$
$$\times[\Theta_1'\exp(i\kappa_1'\theta)+\Theta_2'\exp(i\kappa_2'\theta)]$$
$$\times\exp(i\omega t). \qquad (32)$$

そして，(32) において $k=\omega$ の場合には，解は (25) と同一の型をとることになる。いずれにしても，境界条件によって，海岸線沿いの進行性の波があらわれたり，定在波があらわれたりすることになる。

4. 凸海岸における波

海岸線が海に向かって凸である場合，水深 h が沖へ向かって海岸線 ($r=r_0$) からの距離 ($r-r_0$) に比例して深くなっていくとき，

$$h=-\alpha(r-r_0),\quad r\geqq r_0. \qquad (33)$$

ここに，α は正の実定数とする。式の形からみて，前節の (8) で (r_0-r) を $(r-r_0)$ に，α を $-\alpha$ に書きかえると，ここで必要な式が得られることになる。すなわち，前節の (14) に対応するものとして，

$$\left.\begin{aligned}&i\omega\frac{r^2}{R}\frac{d^2R}{dr^2}+\frac{i\omega r^2}{r-r_0}\frac{1}{R}\frac{dR}{dr}-\frac{\alpha_0 r^2}{r-r_0}\\&\qquad=ik,\\&\frac{i\omega}{\Theta}\frac{d^2\Theta}{d\theta^2}+\frac{f}{\Theta}\left(\frac{r}{r-r_0}-1\right)\frac{d\Theta}{d\theta}=ik.\end{aligned}\right\} \qquad (34)$$

ここでは，やはり，(C) r_0 が十分大きな場合と (D) r_0 が十分小さな場合とが考えられる。

(C) r_0 が十分大きい場合 ($r_0\to\infty$)，(34) の第2式で

$$\left(\frac{r}{r-r_0}-1\right)\to-1 \qquad (35)$$

であるから，

$$s=r-r_0 \qquad (36)$$

なる書きかえをすると (34) は

$$\left.\begin{aligned}&\frac{d^2R}{ds^2}+\frac{1}{s}\frac{d^2R}{ds}-\left(\frac{\alpha_0}{s}+\frac{ik}{(r_0+s)^2}\right)\frac{R}{i\omega}\\&\qquad=0,\\&\frac{d^2\Theta}{d\theta^2}-\frac{f}{i\omega}\frac{d\Theta}{d\theta}-\frac{k}{\omega}\Theta=0.\end{aligned}\right\} \qquad (37)$$

ただし，

$$\alpha_0=-\frac{(f^2-\omega^2)i\omega}{g\alpha}.$$

ここで，(37) の第1式で r_0 が十分大きいとして，漸近的に

$$\frac{d^2R}{ds^2}+\frac{1}{s}\frac{dR}{ds}-\frac{\alpha_0}{i\omega s}R=0 \qquad (38)$$

この式の解は

$$R=R_1\cdot Z_0\left(\pm2\sqrt{\frac{\omega^2-f^2}{g\alpha}(r-r_0)}\right) \qquad (39)$$

さらに，(37) の第2式は (18) の第2式と同じであるから，とくに $C=0$ の場合，もとむる解は

$$\zeta=R_1\cdot J_0\left(2\sqrt{\frac{\omega^2-f^2}{g\alpha}(r-r_0)}\right)$$
$$\times[\Theta_1\exp(i\kappa_1\theta)+\Theta_2\exp(i\kappa_2\theta)]\cdot e^{i\omega t}. \qquad (40)$$

前節におけると同様に考えて，ω が f より大きいと ζ の r に対する変化はベッセル関数 J_0 で特長づけられるが，ω が f より小さいときは変形ベッセル関数 I_0 で特長づけられることになる。

(D) r_0 が十分小なる場合 ($r_0\ll r$)，漸近的な式として

$$\left.\begin{aligned}&\frac{d^2R}{ds^2}+\frac{1}{s}\frac{dR}{ds}-\frac{\alpha_0 s+ik}{s^2}\frac{R}{i\omega}=0\\&\frac{d^2\Theta}{d\theta^2}-\frac{k}{\omega}\Theta=0\end{aligned}\right\} \qquad (41)$$

が導びかれる。ここに，(41) の第1式の解は

$$R=R_1'\cdot Z_{4k/\omega}\left(\pm\sqrt{\frac{-4\alpha_0}{i\omega}(r-r_0)}\right) \qquad (42)$$

あるいは

$$R=R_1'\cdot Z_{4k/\omega}\left(\pm\sqrt{\frac{\omega^2-f^2}{g\alpha}(r-r_0)}\right) \qquad (43)$$

そして，(41) の第2式の解は

$$\Theta=\Theta_0\exp(i\kappa\theta)+\Theta_0'\exp(-i\kappa\theta)\quad(44)$$

したがって，とくに $C=0$ の場合

$$\zeta=R_1'\cdot\left[J_{4k/\omega}\left(2\sqrt{\frac{\omega^2-f^2}{g\alpha}}(r-r_0)\right)+R_2'\cdot J_{-4k/\omega}\left(2\sqrt{\frac{\omega^2-f^2}{g\alpha}}(r-r_0)\right)\right]\times[\exp(i\kappa\theta)+\Theta_1'\exp(-i\kappa\theta)]\cdot\exp(i\omega t)\quad(45)$$

が所要の解となる。この解で，ζ の r に対する特長は，ω が f より大きいときはベッセル関数であるが，ω が f より小さいときは変形ベッセル関数で特長づけられることになる。ここに，

$$J_\nu(zi)=i^\nu I_\nu(z).$$

海岸線に沿った距離 $r\theta$ の θ は，円弧状海岸線のひろがりによって定まり，海岸線の両端での θ_1 および θ_2 について，$0<|\theta_1-\theta_2|<2\pi$ と考えてよい。とくに，$\theta_1=\theta_2$ の場合は，島のまわりの波と考えることができる。

5. 水槽実験で可能とみられる波

普通の波の実験水槽は小規模であり，地面に相対的に固定されている。このような場合には，前節までに考えたコリオリの効果は考慮にいれる必要がないとみて差支えない。前節までの分類にしたがって，非回転系について得られる解は，つぎのように書ける。

(A) 凹海岸で $r_0\to\infty$ の場合，

$$\zeta=R_0\cdot s\cdot I_0\left(2\sqrt{\frac{\omega^2 s}{g\alpha}}\right)\times[\Theta_1\exp(i\kappa_1\theta)+\Theta_2(i\kappa_2)]\cdot\exp(i\omega t).\quad(46)$$

(B) 凹海岸で $r_0\ll r$ の場合，

$$\zeta=R_1\cdot s\cdot i^{4(1-k/\omega)}\left[I_{4(1-k/\omega)}\left(2\sqrt{\frac{\omega^2 s}{g\alpha}}\right)-R_2\exp\left\{4\left(1-\frac{k}{\omega}\right)\pi i\right\}\cdot I_{-4(1-k/\omega)}\left(2\sqrt{\frac{\omega^2 s}{g\alpha}}\right)\right]\times[\Theta_1'\exp(i\kappa_1'\theta)+\Theta_2'\exp(i\kappa_2'\theta)]\cdot\exp(i\omega).\quad(47)$$

とくに，$k=\omega$ のとき，(47) は (46) と同一型となる。そして，(46) および (47) を (25) および (32) と比較してみると，海岸線から沖方向の波高分布にあらわれる地球自転の効果の差異を知ることができる。

(C) 凸海岸で $r_0\to\infty$ の場合，

$$\zeta=R_1'\cdot J_0\left(2\sqrt{\frac{\omega^2 s}{g\alpha}}\right)\cdot[\Theta_1\exp(i\kappa_1\theta)+\Theta_2\exp(i\kappa_2\theta)]\cdot\exp(i\omega t).\quad(48)$$

(D) 凸海岸で $r_0\ll r$ の場合，

$$\zeta=R_1'\cdot\left[J_{4k/\omega}\left(2\sqrt{\frac{\omega^2 s}{g\alpha}}\right)+R_2'J_{-4k/\omega}\left(2\sqrt{\frac{\omega^2 s}{g\alpha}}\right)\right]\times[\Theta_1''\exp(i\kappa\theta)+\Theta_2''\exp(i\kappa\theta)]\cdot\exp(i\omega t)\quad(49)$$

ということになる。(49) は $k=\omega$ の場合，(48) と同一型をとる。そして，(48) は，直線状海岸での波に漸近的に一致するものとみられる。

地球自転の効果によってあらわれるような波について実験を試みるためには，地面に相対的に固定した水槽を用いて，(46)-(49) のいずれかを検討するよりも，人為的に回転させた水槽を用いて，(25)，(32)，(40) あるいは (45) のいずれかについて検討することがより妥当と考えられる。

海底こう配の効果は，ここで考えた解のいずれの例でも，海岸線から沖方向への波高分布にあらわれている。また，考える波の周波数も，海岸線から沖方向の波高分布に影響を与えることも，それぞれの解の型からわかる。

円弧状海岸線に沿ってみられる線型波について，厳密解を得ることはできなかったけれども，基礎方程式を漸近的線型微分程式に誘導し，可能な波の特長をとらえることができたものと考えられる。

文　献

1) 中村重久（1976a）：線型解としてみたエッジ波，うみ；日仏海洋学会誌，**14**, 1-6.
2) 中村重久（1976b）：外力の作用による線型エッジ波，うみ；日仏海洋学会誌，**14**, 139～143.
3) 犬井鉄郎（1962）：特殊関数，岩波全書，No. 252，岩波書店，東京，p. 1-376.

La mer (Bulletin de la Société franco-japonaise d'océanographie)
Tome 17, N° 1, pp. 33 à 42, Février 1979

Eunicid Polychaetous Annelids from Japan—III*

Tomoyuki MIURA**

Résumé: Cinq espèces appartenant aux genres *Eunice*, *Marphysa* et *Nematonereis*, sont décrites. Trois espèces sont nouvelles pour la faune japonaise. *Eunice gracilicirrata* possède des soies aciculaires bidentees de couleur jaune. *E.* cf. *investigatoris* est caractérisé par les branchies développées dans les parapodes antérieurs ainsi que dans les parapodes postérieurs. Deux spécimens juvéniles récoltés à Kominato sont identifiés à *Marphysa conferta*. Les deux espèces *Eunice afra* et *Nematonereis unicornis* sont communes dans les eaux peu profondes de la région indo-pacifique.

1. Introduction

In the present study, five species belonging to the three genera *Eunice*, *Marphysa* and *Nematonereis* are studied. Three of them, *Eunice gracilicirrata*, *E.* cf. *investigatoris* and *Marphysa conferta*, are newly added to the Japanese fauna.

We are deeply indebted to Director Dr. Lucien LAUBIER of the Centre Océanologique de Bretagne, Brest and Dr. Kristian FAUCHALD of Smithsonian Institution, Washington for their critical reading of the manuscript. We wish to express our thanks to Dr. Minoru IMAJIMA of National Science Museum, Tokyo and Professor Dr. Tatsuyoshi MASUDA of Tokyo University of Fisheries, Tokyo for their valuable advice. Thanks are also due to Dr. Kazuhiro KONNO of Hirosaki University, Hirosaki, who donated us some specimens examined in this study.

The collections are deposited in the National Science Museum, Tokyo.

2. Materials and methods

Each specimen examined is presented here under the heading "Material" description of each species. The details for this section are given in a preceding report (MIURA, 1977a).

3. Description

Family Eunicidae SAVIGNY, 1818
Genus *Eunice* CUVIER, 1817

Eunice afra PETERS, 1817
(Fig. 1, a-n)

Eunice afra: CROSSLAND, 1904, pp. 289-296, pl. 20, figs. 1-5; OKUDA, 1937, pp. 276-278, figs. 18-19; HARTMAN, 1944, pp. 110-111, pl. 6, figs. 135-139; OKUDA, 1940, p. 17; IMAJIMA and HARTMAN, 1964, p. 250; FAUCHALD, 1970, pp. 16-18, pl. 1, figs. h-i.

Material

A	B	C	D	E	F	G	H	I	J
E 180	Apr. 17, 1976 Ishigaki	7.5	16-1	200-1	21-1	233	5	6.0	C S
E 181	,,	10.0	16-1	190-1	23-1	207	5	5.5	S C

Description: Two specimens were collected at Kabira, Ishigaki Island, in intertidal dead coral rock.

A complete worm measures 125 mm long by 6.0 mm wide including parapodia with 233 setigers. The body is cylindrical anteriorly with numerous white dots. The fourth setiger

* Received December 15, 1978
** Ocean Research Institute, University of Tokyo, 15-1, Minamidai-1, Nakano-ku, Tokyo, 164 Japan

is colorless (Fig. 1, a). The prostomium is shallowly incised in front. The two oval eyes are outside the inner lateral antennae. The five antennae are irregularly annulated; the central longest one is two and a half times as long as the prostomium and has eight articulations, the inner lateral ones are almost equal to the central in length and in number of articulations, the outer lateral ones are one and a half times as long as the prostomium and have three to five articulations. The first peristomial ring projects forward on both ventro-lateral sides and is three times as long as the second one. A pair of short, irregularly annulated peristomial cirri are

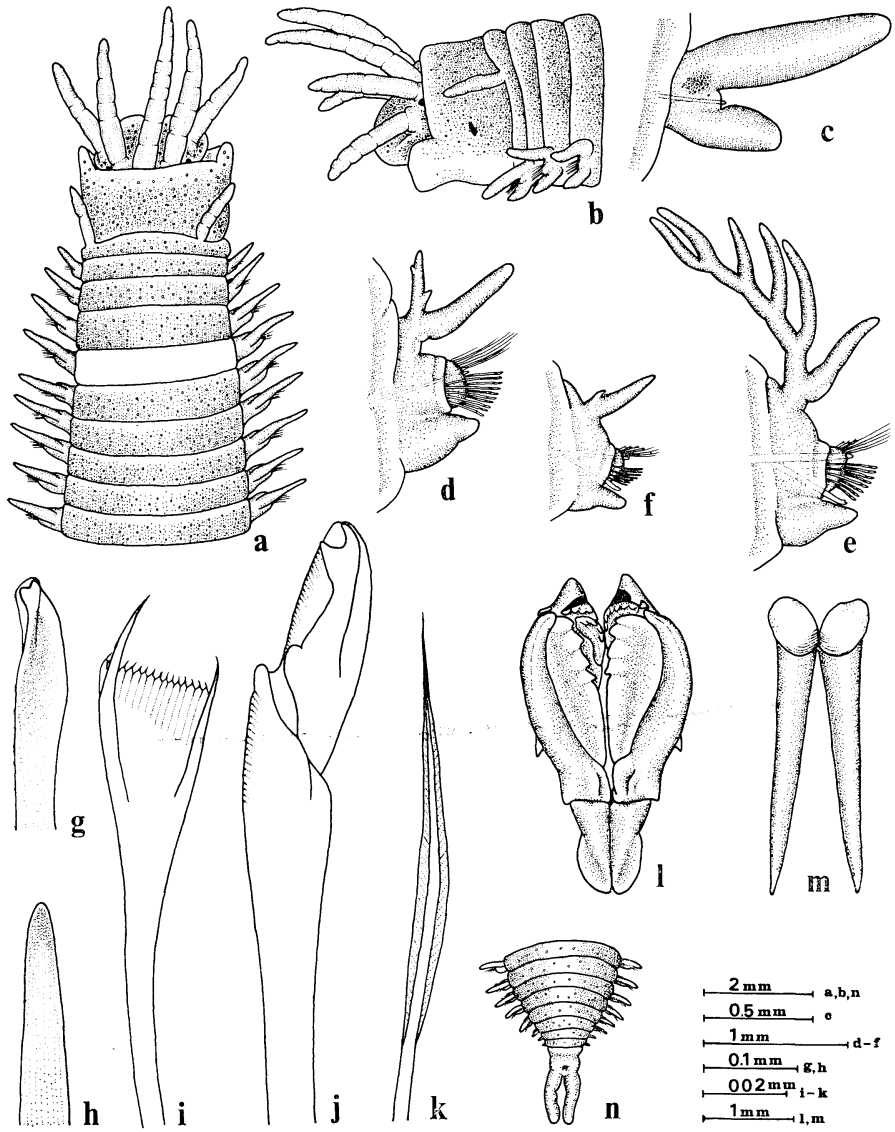

Fig. 1. *Eunice afra* Peters, 1817. a. Anterior end in dorsal view. b, The same, in lateral view. c, First parapodium, in anterior view. d, Parapodium 16. e, Parapodium 49. f, Parapodium 200. g, Subacicular hook. h, Aciculum. i, Pectinate seta. j, Compound falciger. k, Capillary seta. l, Maxillae, in dorsal view. m, Mandibles, in ventral view. n, Posterior end, in dorsal view.

as long as the prostomium (Fig. 1, b).

The ventral cirrus of the first parapodium is simple, digitiform and the dorsal one cylindrical (Fig. 1, c). Several anterior setigers have two acicula per parapodium (Fig. 1, d). Each posterior parapodium has an aciculum and a subacicular hook (Fig. 1, e–f). The rounded setal lobe always projects beyond the presetal lobe. Branchiae start from setiger 16 with a single or more filaments. The number of filaments increases rapidly, the maximal is five at about setiger 50 (Fig. 1, e), then it gradually decreases until the posterior end. The posterior branchial filament forms a simple papilla on the dorsal cirrus (Fig. 1, f).

The dark subacicular hooks are bidentate and hooded (Fig. 1, g). They are first present from setigers 21–23 and occur singly in a parapodium. Both teeth are directed distally. The acicula are stout and have dark blunt ends (Fig. 1, h). Each pectinate seta has asymmetrical extensions and 15 or more inner teeth (Fig. 1, i). The compound falcigers are bidentate and hooded (Fig. 1, j). Both teeth are directed obliquely upward. The cutting margin of each hood has 20–25 serrated minute teeth. The stem has 15–20 rows of short spines. Capillary setae are bilimbate (Fig. 1, k).

The maxillary formula is Mx. I=1+1 (forceps), Mx. II=4+4, Mx. III=(5–6)+0, Mx. IV=3+(6–9), Mx. V=1+1 (Fig. 1, l). The maxillary carriers are twice as long as wide. The mandibles are long and slender with oval calcified bodies (Fig. 1, m). The distal cutting edge has 7–10 lines. The shaft is more than five times as long as wide. The pygidium has two anal cirri (Fig. 1, n).

Discussion: The arrangement of branchia is variable. According to FAUCHALD (1970), *Eunice afra* includes forms with branchiae from setigers 11–20 and a maximum of nine filaments. The Japanese form was noted by IMAJIMA and HARTMAN (1964), as having branchiae from setigers 15–16 and a maximum of six filaments. The specimens from Ishigaki are considered as belonging to *E. afra* especially as described from Japan.

Distribution: Indo-Pacific area and West Indies in shallow waters; Southern Japan.

Eunice gracilicirrata (TREADWELL, 1922)
(Fig. 2, a–r)

Leodice gracilicirrata TREADWELL, 1922, pp. 149–150, figs. 36–38, pl. 5, figs. 1–8.

Material

A	B	C	D	E	F	G	H	I	J
E 193	Apr. 16, 1976 Ishigaki	6.2	3-1	239-1	56-1	343	8	4.2	S C

Description: One complete specimen separated in two pieces was collected at Kabira, Ishigaki Island in intertidal dead coral rock. The two pieces combined measure 140 mm long by 6.0 mm wide with 343 setigers. Some anterior and posterior setigers are cylindrical and the middle ones flattened. The prostomium is bilobed in front. The two small eyes are outside the inner lateral antennae and are nearly triangular with concave upper margins. Prostomial antennae are irregularly annulated; the central one with twelve annulations is two and a half times as long as the prostomium, the inner lateral ones are almost equal to the central, the outer ones with seven to eight annulations are twice as long as the prostomium. Peristomial cirri are long, slender and reach beyond the anterior margin of the prostomium. The first ring is twice as long as the second one (Fig. 2, a). The first one does not project forward on the ventro-lateral sides (Fig. 2, b).

Parapodia are characterized by their very long dorsal cirri. The dorsal cirri are three to five times as long as the ventral cirri. The annulation of dorsal cirri is distinct in the anterior parapodia (Fig. 2, c–e), and indistinct or absent in the remaining parapodia (Fig. 2, h–j). Ventral cirri are digitiform in the anterior few parapodia (Fig. 2, c–d), with proximal pads in the middle parapodia (Fig. 2, e–g), and are simple cones in the posterior parapodia (Fig. 2, h–j). Branchiae start from setiger 3 with single

slender filament (Fig. 2, d). The number of filaments increases rapidly, the maximal number is eight at about parapodium 40, thereafter it decreases gradually and is five at setiger 100.

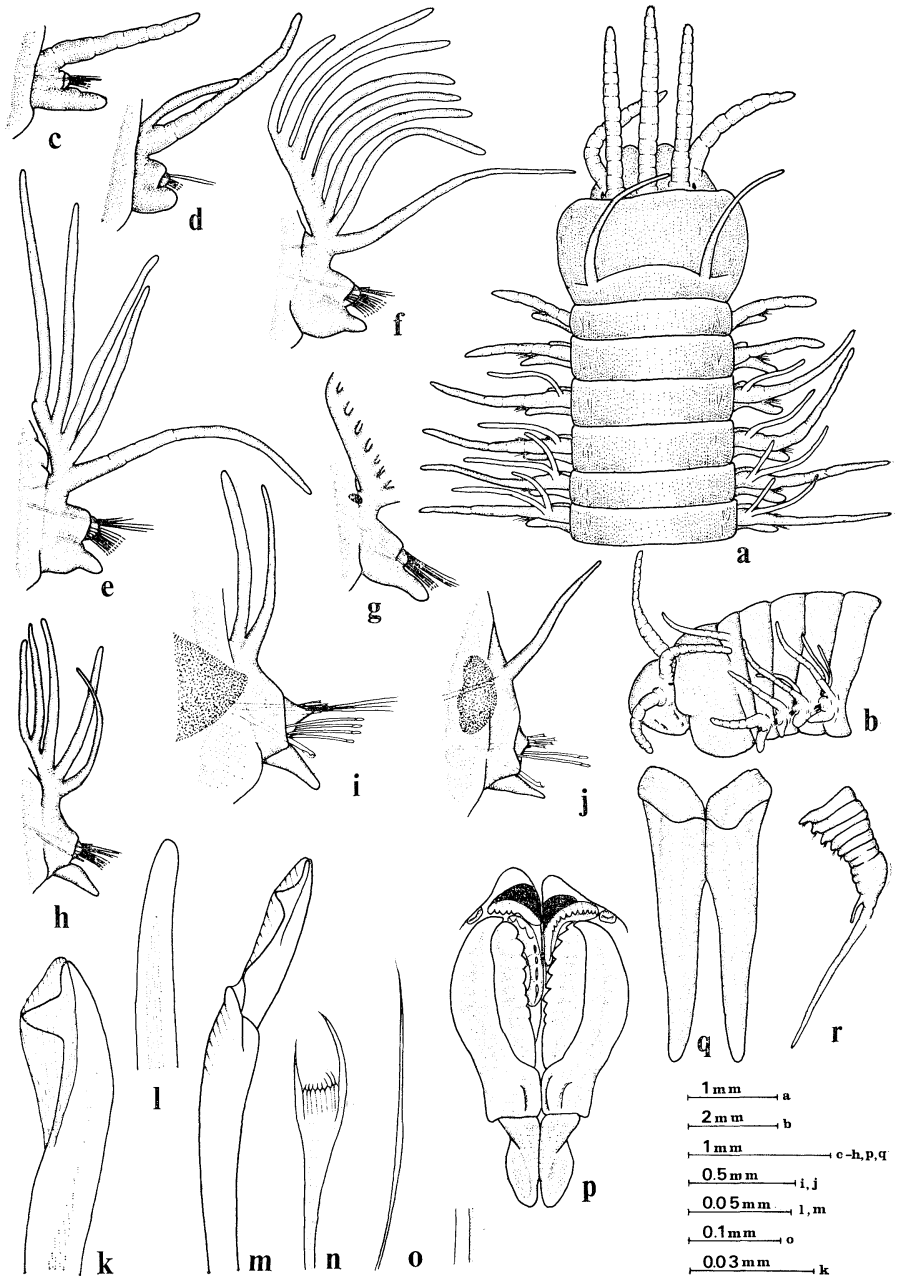

Fig. 2. *Eunice gracilicirrata* (Treadwell, 1923). a, Anterior end, in dorsal view. b, The same, in lateral view. c, First parapodium, in anterior view. d, Parapodium 3. e, Parapodium 15. f, Parapodium 30. g, Parapodium 70. h, Parapodium 120. i, Parapodium 200. j, Parapodium 240. k, Subacicular hook. l, Aciculum. m, Compound seta. n, Pectinate seta. o, Capillary seta. p, Maxillae, in dorsal view. q, Mandibles, in ventral view. r, Posterior end, in lateral view.

four at setiger 120 (Fig. 2, h) and one at setigers 180–240 (Fig. 2, i). Far posterior parapodia lack branchiae (Fig. 2, j).

Yellow subacicular hooks are first present from setigers 56–58 and occur singly in a parapodium. They are bidentate and hooded, the two teeth are equal in size and at right angles to each other (Fig. 2, k). Two yellow acicula occur on each parapodium, their tips are stout, slightly curved and project from the setal lobes (Fig. 2, l). Compound falcigers are bidentate and hooded, the appendage is rather long, the two teeth are widely separated, the hood has six to twelve rows of short spines; the shaft seven to ten rows on the cutting side (Fig. 2, m). Pectinate setae have seven to eight inner teeth and asymmetrical lateral extensions (Fig. 2, n). Capillary setae are slender and limbate (Fig. 2, o).

The maxillary formula is Mx. I=1+1 (forceps), Mx. II=7+8, Mx. III=6+0, Mx. IV=5+10, Mx. V=1+1. The maxillary carriers are concave at the distal ends (Fig. 2, p). The mandibles are stout and rather short, the distal cutting edges have 19–20 lines (Fig. 2, q). The pygidium has two long dorsal and two short ventral cirri, the dorsal one is seven to eight times as long as the ventral one (Fig. 2, r).

Discussion: *Eunice gracilicirrata* resembles *E. armillata* (TREADWELL, 1922) and they have been considered synonymous by HARTMAN (1956). *E. gracilicirrata* has branchiae with a maximal number of seven filaments from setiger 3 to about the 125th parapodium from the pygidium, whereas *E. armillata* has a maximal number of two filaments from setiger 6 to the 10th parapodium from the pygidium. The dorsal cirri of *E. gracilicirrata* are long and slender instead of short and stout as in *E. armillata*. The present author considers that *E. gracilicirrata* is a valid species. The specimen from Ishigaki agrees with *E. gracilicirata* with respects to the branchial distribution and of the shape of dorsal cirri.

Distribution: Suba Harbor, Fiji; Southern Japan.

Eunice cf. *investigatoris* FAUVEL, 1932
(Figs. 3 and 4, a–o)

Eunice investigatoris FAUVEL, 1932, pp. 137–138, fig. 19, a–f.

Material

A	B	C	D	E	F	G	H	I	J
E 216	Fukaura, 30 m depth	22.5	8-3	169-1	40-1	169	23	10.0	A F
E 217	,,	22.0	9-2	163-11	42-1	163	25	10.0	A F

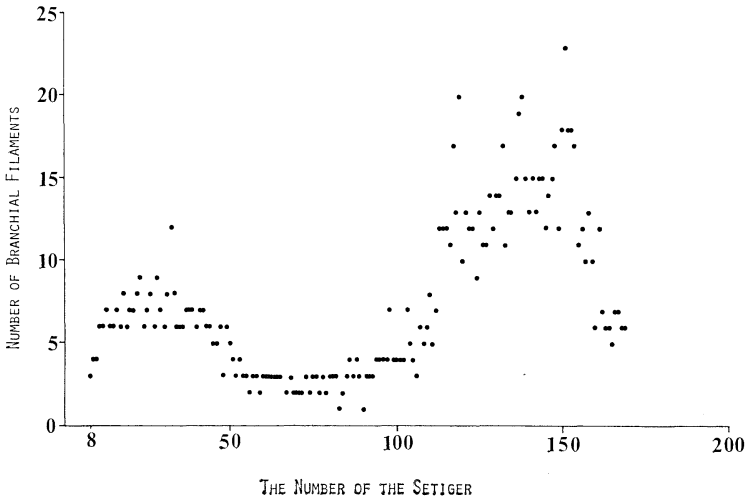

Fig. 3. Branchial distribution in specimen E 216 of *Eunice* cf. *investigatoris* Fauvel, 1932.

Description: Two specimens were collected from Fukaura, North-west coast of Honshu in 30 m depth. Specimen E 216 has a parchment-like tube partially covered with small gravels, and measures 290 mm long by 10 mm wide for 169 setigers. Both specimens lack some caudal

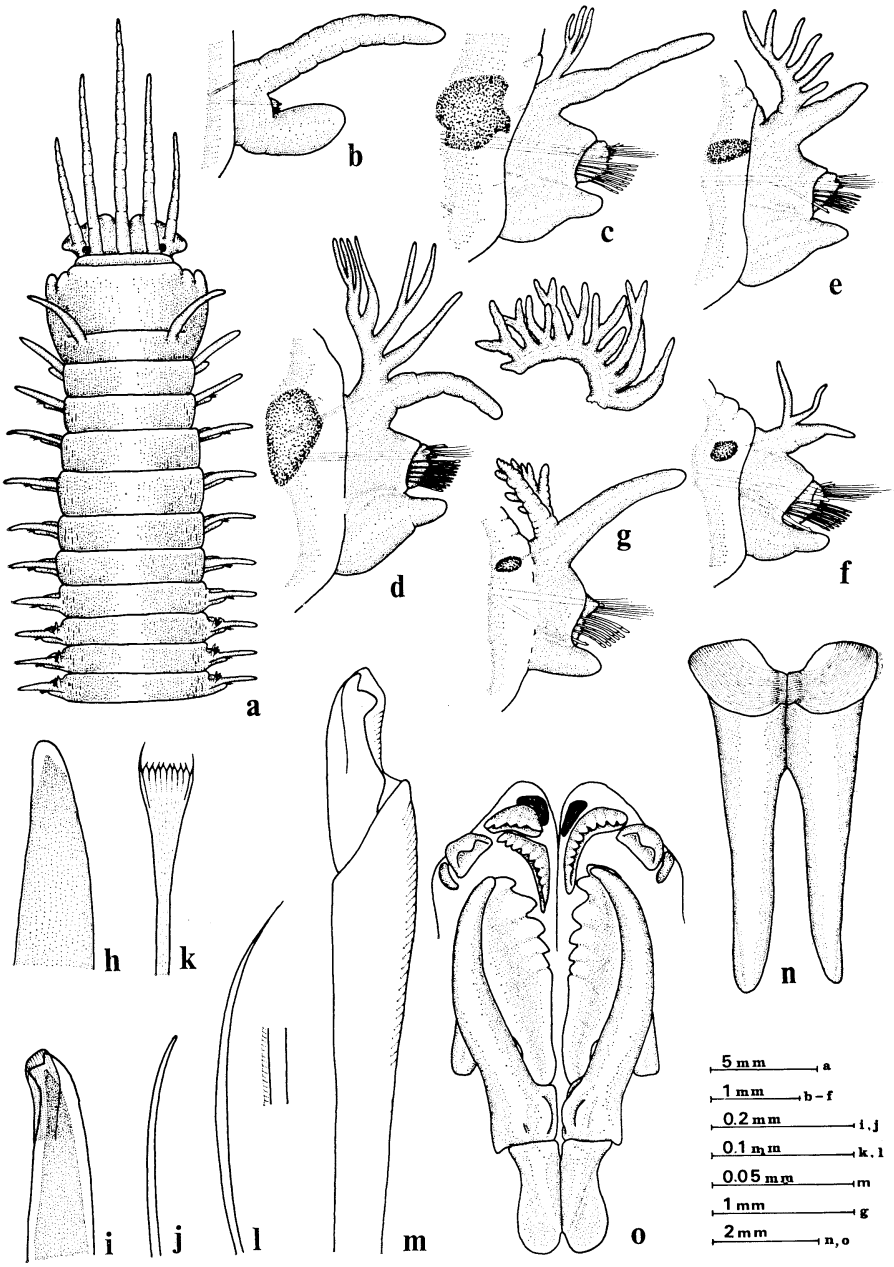

Fig. 4. *Eunice* cf. *investigotoris* Fauvel, 1932. a, Anterior end, in dorsal view. b, First parapodium, in anterior view. c, Parapodium 8. d, Parapodium 20. e, Parapodium 40. f, Parapodium 70. g, Parapodium 150 in anterior view and the branchia in lateral view. h, Aciculum. i, Subacicular hook. j, Notoacicular seta. k, Pectinate seta. l, Capillary seta. m, Compound falciger. n, Mandibles, in ventral view. o, Maxillae, in dorsal view.

segments. The coloration could not be described on alcoholic specimens. The body is cylindrical anteriorly and relatively flattened posteriorly.

The prostomium is deeply notched in front and is twice as wide as long. The two rounded eyes are outside the inner lateral antennae. There are five occipital antennae; the central one with twelve annulations reaches the anterior margin of setiger 4, the inner lateral ones with ten annulations reach the middle of setiger 3, the outer ones with seven to eight annulations reach the anterior margin of the second peristomial ring. The anterior part of the first peristomial ring overlaps the posterior part of the prostomium and is projected forward on lateral sides. The second ring has a pair of cirri as long as the first ring and they have five annulations. The peristomial rings combined are wider than long (Fig. 4, a).

The first parapodium has a cylindrical dorsal cirrus, a digitiform ventral one and a few setae (Fig. 4, b). The dorsal cirri are longer and stouter than the branchial filaments or stems in all branchial setigers. The ventral cirri bear anteriorly basal swellings (Fig. 4, c-f) and are simple and digitiform posteriorly (Fig. 4, g). The setal lobes are rounded with small papillae in the supracicular portion (Fig. 4, c-e). Branchiae are first present from setiger 8 with three filaments (Fig. 4, c). The number of branchial filaments increases to eight to 12 on setigers 26-33, then decreases to one to three on setigers 55-94, thereafter it increases again to 20-23 on setigers 130-154 and decreases again to five to six in the posterior end of the incomplete specimen. The exact distribution of branchial filaments is given in Fig. 3. The branchiae anterior to setiger 100 are directed parallel with the dorsal cirri and the posterior branchiae at a right angle to the cirri (Fig. 4, d-g).

Each parapodium has one to three dark acicula (Fig. 4, h). The subacicular hooks are present from setiger 40 as a single seta. They are dark, bidentate and hooded (Fig. 4, i). Notoacicular setae inside of the base of the dorsal cirrus, are slender and number four to five in a bundle (Figt 4, j). Each pectinate seta has lateral asymmetrical extensions and about eight inner teeth (Fig. 4, k). Capillary setae are long, slender and limbate (Fig. 4, l). Compound falcigers are bidentate and hooded; the hood has 10-12 serrations on the cutting edge, the stem has many short spines in 30-50 rows (Fig. 4, m).

The pharyngeal apparatus is black. The mandibles have stout shafts and the calcified bodies with more than 20 lines (Fig. 4, n). The maxillary supports are long. The maxillary formula is Mx. I=1+1, Mx. II=5+6, Mx. III =8+0, Mx. IV=5+9, Mx. V=1+1 (Fig. 4, o).

Discussion: *Eunice investigatoris* shows a bi-modal distribution of branchiae. Such distribution was mentioned by FAUVEL (1932) for this species and for *E. antennata* (SAVIGNY, 1820). *E. antennata* can be distinguished from this species in that it has yellow, tridentate subacicular hooks.

Branchiae were present from setiger 8 or 9 in our specimens and from setiger 6 in the original material of *E. investigatoris*. The maximal number of branchial filaments on the anterior part is about ten in our specimens and were 18-20 in Fauvel's.

Distribution: Persian Gulf, 45 m; Fukaura, 30 m.

Genus *Marphysa* QUATREFAGES, 1865
Marphysa conferta MOORE, 1911 (juvenile)
(Fig. 5, a-j)

Marphysa conferta MOORE, 1911, pp. 252-254, pl. 16, figs. 29-34; HARTMAN, 1944, p. 129; 1961, p. 83; FAUCHALD, 1970, pp. 59-60.

Material

A	B	C	D	E	F	G	H	I	J
E 198	July 31, 1976, Kominato	1.7	8-4	17-5	18-1	70	5	1.3	S C
E 199	,,	1.7	7-3	16-3	16-1	34	5	1.3	A F

Description: Two juvenile specimens were collected from a subtidal rocky shore of Kominato. They lived in the roots of *Phyllospadix japonica*. A complete specimen measures 4.7 mm long by 1.3 mm wide for 70 seitgers. The body is cylindrical and colorless except for the black eyes. The prostomium is rounded anteriorly and longer than wide. There are three occipital antennae; all of them are smooth and do not reach beyond the anterior margin of the prostomium. The two eyes are outside the paired antennae. The first peristomial ring is U-shaped in dorsal view and slightly longer than the second one (Fig. 5, a).

The dorsal cirri are cylindrical and slender. The ventral cirri have proximal pads. The setal lobes are triangular. The postsetal lobes are conical and higher than the setal lobes in the parapodia anterior to setiger 20. Ten pairs of branchiae are present. They start at setiger 7 or 8 with three to four filaments (Fig. 5, b). The maximal number of filaments is five.

Yellow acicula are present singly in a parapodium (Fig. 5, c). Subacicular hooks are yellow, bidentate and hooded (Fig. 5, d). They start at setigers 16–18 and occur singly in a parapodium. Compound falcigers are bidentate and hooded (Fig. 5, e). Compound spinigers are absent. Each pectinate seta has asymmetrical lateral extensions and six to eight inner teeth (Fig. 5, f). Capillary setae have numerous spines on their cutting margins (Fig. 5, g).

The mandibles have long shafts and their cutting edges have three lines (Fig. 5, h). The maxillary carriers are long and have narrow basal wings. The maxillary formula is Mx. I=1+1, Mx. II=6+6, Mx. III=6+0, Mx. IV=4+10, Mx. V=1+1 (Fig. 5, i). The pygidium has a pair of anal cirri (Fig. 5, j).

Discussion: *Marphysa conferta* as originally described by MOORE (1911) measures 24 mm long for 57 setigers. Our specimens are juvenile in that they have only three antennae. The larger one measures 4.7 mm long for 70 setigers.

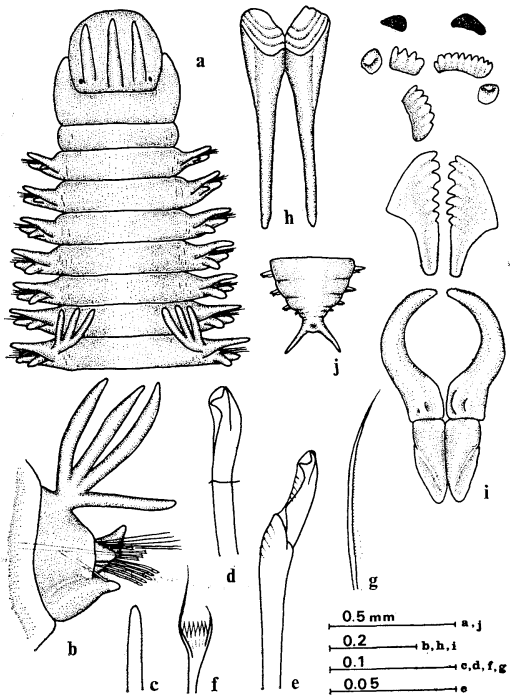

Fig. 5. *Marphysa conferta* Moore, 1911 (juvenile). a, Anterior end, in dorsal view. b, Parapodium 16, in anterior view. c, Aciculum. d, Subacicular hook. e, Compound falciger. f, Pectinate seta. g, Capillary seta. h, Mandibles, in ventral view. i, Maxillae, in dorsal view. j, Posterior end, in dorsal view.

According to FAUCHALD (1970), two species are characterized by the presence of the branchia limited to an anterior region of the body, the presence of compound falcigers and the absence of compound spinigers. *M. adenensis* GRAVIER, 1900 has branchia from setiger 13 to setiger 29. *M. conferta* has branchiae from setiger 8 to setiger 16 (X–XVII after MOORE). The present specimens fit with *M. conferta* in that they have branchiae from setiger 7 or 8 to setiger 16 or 17.

Distribution: off Brockway Point, Santa Rosa Island, 69.5–73.3 m; California; Kominato, Japan.

Genus *Nematonereis* SCHMARDA, 1861

Nematonereis unicornis (GRUBE, 1840)

(Fig. 6, a–g)

Nematonereis unicornis: FAUVEL, 1923, pp. 412-413, fig. 162, h-n; OKUDA, 1937, pp. 290-291, figs. 36-37; 1938, p. 96; IMAJIMA and HARTMAN, 1964, pp. 260-261; IMAJIMA, 1967, pp. 432-433; 1968, p. 31, pl. 12, fig. f; WU *et al.*, 1975, p. 84, fig. 6, 1-9.

Material

A	B	C	D	E	F	G	H	I	J
E 211	July 31, 1976, Kominato	1.4	—	—	11-1	—	23	0.8	A F
E 215	Sep. 7, 1976, Kominato	2.2	—	—	15-1	—	42	0.7	A F

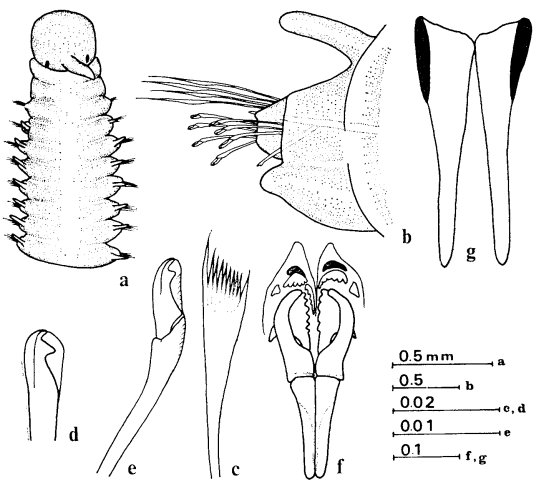

Fig. 6. *Nematonereis unicornis* (Grube, 1840). a, Anterior end, in dorsal view. b, Parapodium 15, in anterior view. c, Pectinate seta. d, Subacicular hook. e, Compound falciger. f, Maxillae, in dorsal view. g, Mandibles, in dorsal view.

Description: Two incomplete specimens were collected from intertidal rocky areas of Kominato. Specimen E 211 measures 3.5 mm long for 23 setigers. The body is filiform. The prostomium is rounded anteriorly with two reddish brown, oval eyes near the posterior margin. There is a smooth occipital antenna shorter than the prostomium. The peristomium consists of two apodous rings (Fig. 6, a). The parapodia are uniramous (Fig. 6, b).

The supracicular setae consist of long capillaries and pectinate setae. Each pectinate seta has nine to ten inner teeth and asymmetrical extensions (Fig. 6, c). Subacicular hooks are bidentate and hooded (Fig. 6, d). They occur singly in a parapodium. The acicula are dark and bluntly tapered. The compound falcigers are bidentate, hooded and distally curved (Fig. 6, e).

The maxillary formula is Mx. I=1+1, Mx. II=6+5, Mx. III=4+0, Mx. IV=5+6, Mx. V=1+1. The maxillary carriers are very long (Fig. 6, f). The mandibles are bigger than the maxillae and not calcified. Each mandible has a dark long support laterally (Fig. 6, g).

Discussion: *Nematonereis unicornis* is a small and common species in the shallow waters of Indo-Pacific area.

WU *et al.* (1975) reported two epitokous specimens collected from Yong-xing Island, the Xisha Islands.

Distribution: Indo-Pacific area; Mediterranean Sea; Japan.

4. Literature cited

CROSSLAND, C., 1904: The Polychaeta of the Maldive Archipelago from the collections made by J. Stanley GARDINER in 1899. Proc. Zool. Soc. London, 1904: 270-286, 2 pls., 5 figs.

FAUCHALD, K., 1970: Polychaetous annelids of the families Eunicidae, Lumbrineridae, Iphitimidae, Arabellidae, and Dorvilleidae from Western Mexico. Allan Hancock Monogr. Mar. Biol., **5**: 1-335, 27 pls.

FAUVEL, P., 1923: Polychètes errantes. Faune de France, **5**: 1-448, 181 pls.

FAUVEL, P., 1932: Annelida Polychaeta of the Indian Museum, Calcutta. Mem. Indian Mus. Calcutta, **12**: 1-262, 9 pls.

GRAVIER, C., 1900: Contribution à l'étude des annélides polychètes de la mer Rouge. Nouv. Arch. Mus. Hist. Nat. Paris, **2**(4): 137-282, 6 pls.

HARTMAN, O., 1944: Polychaetous annelids. Part 5, Eunicea. Allan Hancock Pac. Exped., **10**: 1-181, 18 pls.

HARTMAN, O., 1956: Polychaetous annelids erected by TREADWELL, 1891 to 1948, together with a brief chronology. Bull. Amer. Mus. Nat. Hist., **109**: 234-310, 1 pl.

IMAJIMA, M., and O. HARTMAN, 1964: The polychaetous annelids of Japan. Part 2. Allan Hancock Found. Publ. Occas. Pap., **26**: 239-452, 3 pls.

MIURA, T., 1977a: Eunicid polychaetous annelids from Japan-I. La mer, Tokyo, **15**: 1-20, 6 figs.
MIURA, T., 1977b: Eunicid polychaetous annelids from Japan-II. La mer, Tokyo, **15**: 61-81, 7 figs.
MOORE, J. P., 1911: The polychaetous annelids dredged by the U.S.S. "Albatross" off the coast of southern California in 1904. III. Euphrosynidae to Goniadidae. Proc. Acad. Nat. Sci. Phila., **63**: 238-318, 7 pls.
OKUDA, S., 1937: Polychaetous annelids from the Palau Islands and adjacent waters, the South Sea Islands. Bull. Biogeogr. Soc. Japan, **7**: 257-315, 59 figs.
OKUDA, S., 1940: Polychaetous annelids of the Ryuku Islands. Bull. Biogeogr. Soc. Japan, **10**: 1-24, 9 figs.
TREADWELL, A. L., 1922: Leodicidae from Fiji and Samoa. Pap. Dept. Mar. Biol. Carnegie Inst. Washington, **18**: 127-170, 8 pls.
WU, B., S. SHEN and M. CHEN, 1975: Preliminary report of polychaetous annelids from Xisha Islands, Guangdong Province, China. Stud. Mar. Sin., **10**: 65-104, 10 figs.

日本産イソメ科多毛環虫類—III

三　浦　知　之

要旨: 第1・2報に続き，本報では日本産イソメ科多毛類の分類学的研究を進め，次の3未記録種と2既知種について記載報告する。

Eunice afra は2歯黒色の足刺状剛毛を持ち，ひろくインド・太平洋浅海に知られている。*E. gracilicirrata* は2歯黄色の足刺状剛毛を持つが，石垣島から採集され，日本初記録である。*E.* cf. *investigatoris* は2歯黒色の足刺状剛毛を持ち，また体前後部に双極的に発達した鰓を備えた数少ない種のひとつである。本種は青森県深浦沖から採集され，日本初記録である。*Marphysa conferta* はカリフォルニアから知られている種であり，幼若な個体が千葉県小湊から初めて得られた。*Nematonereis unicornis* は日本沿岸に普通である。

La mer (Bulletin de la Société franco-japonaise d'océanographie)
Tome 17, N° 1, pp. 43 à 52, Février 1979

Biological and Ecological Studies on the Propagation of the Ormer, *Haliotis tuberculata* LINNAEUS

II. Influence of Food and Density on the Growth of Juveniles*

Yasuyuki KOIKE**, Jean-Pierre FLASSCH*** and Joseph MAZURIER***

Résumé: Des expériences d'élevage des jeunes ormeaux européans, *Haliotis tuberculata*, au sujet de l'influence du régime alimentaire et de la densité d'élevage sur la croissance ont été effectuées pendant 112 jours (du 30 avril au 20 août, 1975) au Centre Océanologique de Bretagne, CNEXO, à Brest, France.

Pour l'alimentation des jeunes ormeaux, les trois espèces d'algue commune sur la côte bretonne ont été utilisées en expérience par espèce ou en conditions de matériaux mélangés, et à l'état frais ou séché, ainsi que les deux types d'aliment artificiel.

La densité du naissain dans un bac d'élevage a été choisie en six étapes de 83 à 5000 par mètre carré de pièce.

Les trois espèces d'algue fraîche (*Rhodymenia palmata, Ulva lactuca, Laminaria digitata*) sont utilisables pour l'alimentation des jeunes. Mais *Rhodymenia palmata* s'avère l'espèce la plus efficace à l'état frais et la seule qui convient à l'état séché.

L'aliment artificiel est efficace pour la croissance des jeunes, mais il serait souhaitable pour l'élevage intensif, qu'il conserve sa forme et ses qualités pendant quelques jours.

La densité convenable en cas d'élevage intensif est estimée entre 2500/m^2 et 3750/m^2.

1. Introduction

The techniques for the artificial propagation of juvenile abalones have been developed in the last ten years in Japan and presently one-year-old juveniles are produced in great numbers and released in many regions. Nevertheless it appears that the commercial demand for juveniles is also increasing.

Concerning the mass production of abalone juveniles, for the period from the spawn to the seedlings for restocking, it is generally completed in one year. During this process, there are many problems which still remain to be solved from the view point of mariculture, for instance, the prime cost of production or the possibility of the condensed rearing.

* Received December 11, 1978
** Centre Océanologique de Bretagne (Aquaculture), CNEXO, 29273-Brest cedex, France
Present address: Laboratory of Animal Ecology, Tokyo University of Fisheries, Minato-ku, Tokyo, 108 Japan
*** Centre Océanologique de Bretagne (Aquaculture), CNEXO 29273-Brest cedex, France

Reports have been given concerning the food and rearing density for juveniles or young abalones which are very important factors for mass production. INO (1952), SAKAI (1962), KIKUCHI (1964), KIKUCHI *et al.* (1967) and SHIBUI (1972) showed the influence of various algae on the growth of juveniles and young *Haliotis discus discus* and *H. discus hannai*. OGINO and OHTA (1963), OGINO and KATO (1964) and SAGARA and SAKAI (1974) carried out experiments on the artificial diet for *H. discus discus* and *H. sieboldii*. TOYAMA *et al.* (1975) examined the most suitable rearing density for the mass production of young *H. discus discus*.

As for the ormer, *H. tuberculata*, in Europe trials for the mass production of juveniles were started in 1973 at Centre Océanologique de Bretagne (CNEXO-COB) in France. And basic studies of larval development and growth of juveniles up to 14 months were published in a previous report (KOIKE, 1978).

The present authors carried out tank rearing experiments of 4-month-old ormer juveniles for 112 days (Apr. 30–Aug. 20, 1975) at the

Centre Océanologique de Bretagne, with a view to examining the influence of food and density on the growth of juveniles. This study reveals some interesting facts new to science.

2. Material and methods

The juveniles used for the experiments originated from artificial spawning at the Centre. They were born in December 1974 and reared with *Tetraselmis suecica* and diatoms until April 1975. Their average size was 7.2 mm in shell length.

Tanks used for experiments were made of polyethylene, rectangular in shape, and 60×40 ×25 cm in size. Each tank was supplied with filtered running water and aeration. The water temperature (20°C±0.5°C), current (1 *l*/min.) and aeration (0.4 *l*/min.) were kept constant throughout the experiments. The openings of the issue pipes were covered with nets with a mesh size of 450 μ so as to prevent juveniles as well as foods from escaping. Pieces of vinyl chloride pipe (12 cm in diameter, 10 cm long) were cut into quarter sections and were used as shelters for the juveniles.

Table 1. Composition of artificial diets.

Artificial diet No. 1

Tetraselmis suecica	60 %
Sodium alginate	20 %
Dextrin (α starch)	15 %
Dried yeast	2 %
Vitamin mixture	2 %
Mineral mixture	1 %

Artificial diet No. 2

Extract of soya bean	
Dried yeast	
Wheat germ	
Bran	
Medicago spp.	
Skim-milk	
Roughage	
Vegetable oil	
Mineral mixture	
Vitamin mixture	
Protein	21 %
Cellulose	3.5 %
Lipid	3.5 %
Mineral	17 %

Table 2. Rearing conditions (food and density).

Food

Name of food	Abbreviation	No. of ormers
Rhodymenia, fresh	Rf	150
Rhodymenia, dry	Rd	,,
Ulva, fresh	Uf	,,
Ulva, dry	Ud	,,
Laminaria, fresh	Lf	,,
Laminaria, dry	Ld	,,
Rhodymenia+*Ulva*+ *Laminaria*, fresh	Mf*	,,
Rhodymenia+*Ulva*+ *Laminaria*, dry	Md	,,
Artificial diet No. 1	A1	,,
Artificial diet No. 2	A2	,,

Density

Items	D0	D1*	D2	D3	D4	D5
No. of ormers	20	150	300	600	900	1250
Density (No/m^2)	83	625	1250	2500	3750	5000

* Same rearing condition (Mf=D1)

Three species of algae were used for the food of the juveniles; *Laminaria digitata* (Phaeophyta) which occurs below the level of mean-low-water neaps, *Rhodymenia palmata* (Rhodophyta) which occurs mainly at the level of mean-low-water neaps and *Ulva lactuca* (Chlorophyta) which is widely distributed in the middle littoral zone. They were fed to the juveniles in both fresh and dried forms, either individually or mixed. In addition, two artificial diets were prepared as shown in Table 1. No. 1 is a modification in composition of the artificial diet tested by OGINO and KATO (1964) in which the fish meal (60 %) was replaced by dried *Tetraselmis suecica*. No. 2* was produced by Mr. J. J. SABAUT of G. I. E. E. R. N. A., Service Pisciculture-Aquaculture.

For the experiments of rearing density, six densities were chosen in the range of 83/m^2 −5000/m^2. The juveniles were fed with the above-mentioned three species of fresh algae in mixed.

All the different experimental conditions are shown in Table 2. A total of 15 different conditions were separated into 15 sections.

* Further detail in composition rate of materials was not informed to the authors.

Furthermore, another 15 sections having the same food and density conditions (abbreviations with prime mark in Fig. 2) were prepared and were placed in the reverse order so as not to have big differences in natural light intensity (Figs. 1 and 2).

Shell length and body weight of the juveniles were measured every two weeks during the experiments. The sample numbers to be measured were calculated as follows:

When a random sample $x(x_1, x_2, \ldots, x_n)$ is taken from a finite population N without replacement and the population variance is unknown, the confidence interval of the population mean at the level of confidence coefficient $1-\alpha$ is $[\bar{x}-\varepsilon, \bar{x}+\varepsilon]$,

$$\text{where} \quad \varepsilon = t_{n-1}(\alpha)\sqrt{\frac{N-n}{N-1}\cdot\frac{u^2}{n}}, \qquad (1)$$

$$\bar{x}=\frac{1}{n}\sum_{i=1}^{n}x_i, \quad u^2=\frac{1}{n-1}\sum_{i=1}^{n}(x_i-\bar{x})^2.$$

The formula (1) can be solved for n;

$$n=\frac{t^2_{n-1}(\alpha)\cdot N\cdot u^2}{\varepsilon^2(N-1)+t^2_{n-1}(\alpha)\cdot u^2}. \qquad (2)$$

As u^2 obtained from the preliminary sampling was between 1.0^2 and 2.0^2, we take 2.0^2 for u^2; moreover, when $\alpha=10\,\%$, $t_{n-1}(\alpha)=1.65$ and $\varepsilon=0.5$ mm.

Therefore, $$n\fallingdotseq\frac{10N}{\frac{N}{4}+10}. \qquad (3)$$

From the formula (3), the numbers of the sample are determined as follows:

$n=20$ from the tanks of 20 juveniles
$n=30$ from the tanks of 150 juveniles
$n=40$ from the tanks of more than 150 juveniles

Food was given every two days at 16 h 00 after its weight and the weight of any remaining food had been measured. The values based on the results of these measurements are expressed as follows;

$$\text{Daily rate of feeding}\,(\%)=\frac{2(F1-F2\pm C)}{T\times(W_0+Wt)}\times 100,$$

where $F1$ is initial weight of food, $F2$ weight of remaining food, C corrective value (increase or decrease in weight of food for experimental conditions with no juveniles), T days of rearing, W_0 initial weight of juveniles and Wt final weight of juveniles.

$$\text{Efficiency of food conversion}\,(\%)=\frac{\text{Increment of weight}}{\text{Total food consumption}}\times 100.$$

The values are expressed after the weights of both food and juveniles have been converted to dry weight.

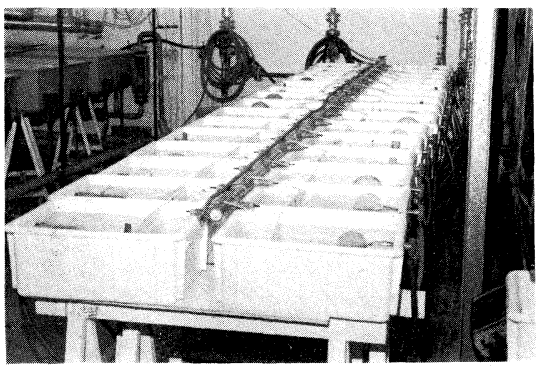

Fig. 1. A set of experimental tanks.

3. Results

1. Influence of food

1-A. Mortality

The number of dead ormers and the mortality rates are shown in Table 3. The mean mortality rates taken on the 14th and 28th day

Ld	Rf	Ud	A2	Md	D0	D2	D3	D4	D5	D1	A1	Uf	Rd	Lf
2400	2600	2600	2200	1850	1500	1200	850	700	600	500	480	440	420	360
Lf′	Rd′	Uf′	A1′	D1′	D5′	D4′	D3′	D2′	D0′	Md′	A2′	Ud′	Rf′	Ld′
1600	1700	1700	1500	1300	1050	1000	1150	700	600	500	460	440	380	380

Fig. 2. Arrangement of the tanks. See Table 2 for abbreviation of food. Figures show the intensity of light in lux over each tank measured on the 20th June at 16 h 00.

Table 3. Number of dead ormers under different food conditions during the experiment. See Table 2 for abbreviation of food.

Days \ Food	Rf	Uf	Lf	Mf	Rd	Ud	Ld	Md	A1	A2	Total	Mortality (%)
0- 14	10	11	10	7	35	10	18	8	15	—	124	4.6
15- 28	5	15	12	7	5	7	13	8	20	—	92	3.4
29- 41	0	8	1	1	5	3	0	6	4	—	28	1.0
42- 56	1	1	1	0	0	1	2	1	0	2	9	0.3
57- 70	0	0	0	2	0	0	0	0	1	2	5	0.2
71- 84	0	1	1	3	3	0	0	1	2	3	14	0.5
85- 98	0	0	1	0	0	1	2	3	1	0	8	0.3
99-112	1	0	0	0	0	2	0	0	2	0	5	0.2
Total	17	36	26	20	48	24	35	27	45	7	285	9.5
Mortality in group (%)		8.3				11.2				8.7	—	—

Table 4. Mean shell length (mm) of young *Haliotis tuberculata* reared under different food conditions during 112 days. See Table 2 for abbreviation of food.

Date and days \ Food		Rf	Uf	Lf	Mf	Rd	Ud	Ld	Md	A1	A2
Apr. 30, '75	0	7.07	7.27	7.19	7.12	6.99	7.38	7.03	7.22	7.49	—
May 14	14	7.62	7.52	7.55	7.67	7.45	7.51	7.30	7.57	7.54	—
May 28	28	8.16	7.95	8.15	7.89	7.84	8.16	7.61	7.85	7.86	—
Jun. 10	41	8.96	8.75	8.74	9.13	8.68	8.65	7.75	8.40	8.51	9.00
Jun. 25	56	10.13	9.68	9.26	9.80	9.37	8.69	7.94	9.67	8.89	9.60
Jul. 9	70	11.35	10.57	10.56	11.15	10.49	9.55	8.52	10.37	9.46	11.11
Jul. 23	84	12.49	11.81	10.79	12.29	11.37	10.54	9.22	11.07	10.24	12.14
Aug. 6	98	13.75	12.47	12.02	13.24	11.99	11.18	9.82	11.66	11.20	13.45
Aug. 20	112	14.58	13.57	12.86	13.95	13.64	12.14	10.15	12.87	12.12	14.11

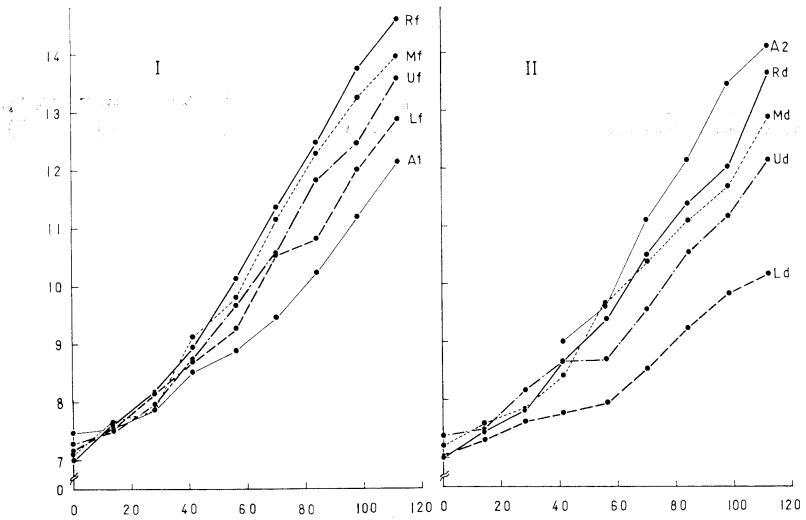

Fig. 3. Growth in shell length (ordinate, mm) of young *Haliotis tuberculata*, reared under different food conditions (cf. Table 2) during 112 days (abscissa). I: Ormers fed on fresh seaweeds and artificial diet No. 1. II: Ormers fed on dried seaweeds and artificial diet No. 2.

Table 5. Rate of growth in shell length and body weight of young *Haliotis tuberculata* reared under different food conditions. See Table 2 for abbreviation of food.

Items / Food	Initial shell length (mm)	Increment of shell length (mm)	Monthly growth rate in shell length (%)	Initial body weight (mg)	Increment of body weight (mg)	Monthly growth rate in body weight (%)	Daily rate of feeding (%)*	Efficiency of food conversion (%)*
Rf	10.13	4.45	23.5	156.5	325.0	111.3	1.8	105.4
Uf	9.68	3.89	21.5	140.0	238.5	91.3	4.1	43.0
Lf	9.26	3.60	20.8	115.0	191.5	89.2	2.2	76.3
Mf	9.80	4.15	22.7	148.0	264.5	95.7	4.4	39.4
Rd	9.37	4.27	24.4	125.0	260.0	111.4	2.0	141.8
Ud	8.69	3.45	21.3	108.0	151.5	75.1	3.7	42.9
Ld	7.94	2.21	14.9	70.0	83.5	63.9	4.1	32.9
Md	9.67	3.20	17.7	133.5	178.5	71.6	—	—
A1	8.89	3.23	19.5	99.5	158.5	85.3	—	—
A2	9.60	4.51	25.2	136.5	320.5	125.8	1.9	103.8

* Converted into dry weight

were 4.6 and 3.4 % respectively, but the rate decreased gradually and kept constant at less than 1 % during the 56th-112th day. The mortality with fresh algae (8.3 %) was lower than that with dried algae (11.2 %), and the mortality with artificial diet (8.7 %) was in between.

1-B. Growth of juveniles

The results of the measurement of shell length and growth are shown in Table 4 and Fig. 3. The final shell lengths for each of the food conditions varied from 10.2 mm (*Laminaria*, dry) to 14.6 mm (*Rhodymenia*, fresh) compared with the initial shell lengths ranging from 7.0 to 7.5 mm. From the results of these measurements, it was found that the rates of growth before and after the 56th day were not the same and the relationship between time in days (T) and shell length (SL) was calculated, e.g. in the case of juveniles fed on fresh *Rhodymenia*:

$SL = 0.044T + 6.930$ (0-56th day)

$SL = 0.078T + 10.313$ (56th-112th day)

This tendency was apparent for juveniles reared under all of the food conditions. From this tendency and the rate of mortality, it can be considered that juveniles needed about 2 months to adapt themselves to the changes of food and environment. Therefore, the feeding values were compared using the results of measurements obtained during the 56th-112th day, that is to say, for the period after adaptation.

1-C. Foods and feeding rate of juveniles

Daily rate of feeding is shown in Table 5. The highest rate (%) with fresh algae was for Mixed (4.4), followed by *Ulva* (4.1), *Laminaria* (2.2) and *Rhodymenia* (1.8). The highest rate with dried algae was for *Laminaria* (4.1), followed by *Ulva* (3.7) and *Rhodymenia* (2.0). The order of *Laminaria* and *Ulva* for fresh and dried conditions was reversed. A comparison between the fresh and dried conditions of the same algae showed that the feeding rate with fresh was higher than with dry in the case of *Ulva* and opposite were the cases of *Rhodymenia* and *Laminaria*. The feeding rate with artificial diet No. 2 was low (1.9), about the same level as that with *Rhodymenia*. In the cases of artificial diet No. 1 as well as Mixed dry, amount of the leftover could not be measured exactly so that feeding rates were not calculated.

1-D. Growth rate of juveniles and efficiency of food

The rates of growth in shell length and body weight were calculated as monthly rates and are shown in Table 5 and Fig. 4 together with the efficiency of food conversion.

The highest rate of growth (%) in shell length with algae in both fresh and dried conditions was for *Rhodymenia* (fresh, 23.5; dried, 24.4), followed by *Ulva* (21.5; 21.3) and *Laminaria* (20.8; 14.9). The growth rate for mixed algae was lower than that for the species which gave the highest rate when fed independently. The rate of growth in shell length was higher with artificial diet No. 2 (25.2) than with No. 1 (19.5). Moreover, it was higher than that for dry *Rhodymenia* (24.4) which gave the highest rate among the algae.

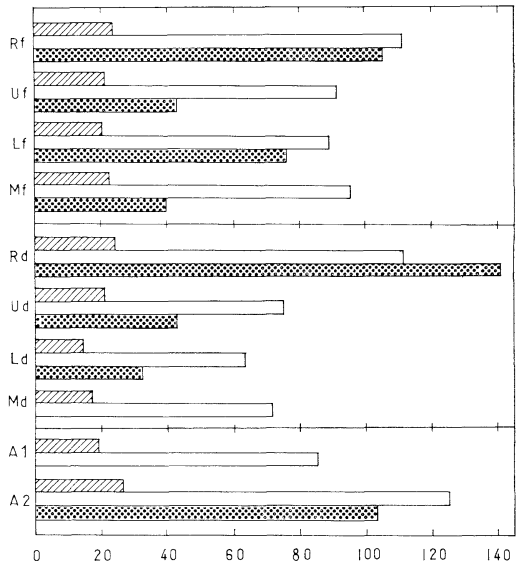

Fig. 4. Comparison of the monthly growth rate (abscissa, %) in shell length (hatched) and body weight (white), and the efficiency of food conversion (dotted) of young *Haliotis tuberculata* reared under different food conditions (ordinate; cf. Table 2).

The rates of growth (%) in body weight with different foods followed the same tendency as in the case of shell length; the highest was for *Rhodymenia* (111.3; 111.4), followed by *Ulva* (91.3; 75.1) and *Laminaria* (89.2; 63.9). The rate for artificial diet No. 2 (125.8) was also superior to that for dry *Rhodymenia* (111.4) which gave the highest rate among the algae tested.

The efficiency of food conversion (%) in the case of fresh algae was highest for *Rhodymenia* (105.4), followed by *Laminaria* (76.3) and *Ulva* (43.0), and lowest for Mixed (39.4). In the case of dried algae, it was also highest for *Rhodymenia* (141.8), followed by *Ulva* (42.9), and lowest for *Laminaria* (32.9). The efficiency of artificial diet No. 2 was very high (103.8) and nearly the same as that for fresh *Rhodymenia* (105.4).

2. Influence of density

2-A. Mortality

The numbers of dead ormers and the mortality rates are shown in Table 6. The mean mortality rates taken on the 14th and 28th day were 3.0 and 3.2 % respectively, but the rate decreased gradually and kept constant at less than 1 % during the 56th-112th day. It is clear that the mortality rate showed the same tendency as that for food condition. In comparisons among the different densities, the mortality rates were higher at densities of 83/m^2 (20 %) and 3750/m^2 (15.4 %) than at the other densities at which the rates were all less than 10 %, and no special relationship was observed between

Table 6. Number of dead ormers under different density conditions during the experiment. See Table 2 for the definition of density.

Days \ Density	D0	D1	D2	D3	D4	D5	Total	Mortality (%)
0- 14	3	7	31	34	84	34	193	3.0
15- 28	4	7	21	16	80	73	201	3.2
29- 41	1	1	3	8	49	31	93	1.5
42- 56	0	0	0	1	27	18	46	0.7
57- 70	0	2	0	2	11	6	21	0.3
71- 84	0	3	2	3	9	16	33	0.5
85- 98	0	0	1	1	16	13	31	0.5
99-112	0	0	0	3	1	1	5	0.1
Total	8	20	58	68	277	192	623	9.8
Mortality (%)	20	6.7	9.7	5.7	15.4	8.0	—	—

mortality and density.

2-B. Density and growth of juveniles

The growths in shell length at different densities are shown in Table 7 and Fig. 5. The final shell lengths varied with different densities between 14.5 mm (83/m²) and 13.1 mm (5000/m²), and the growth rates between the 98th and 112th day for the higher densities (3750/m², 5000/m²) were comparatively lower than those for the lower densities.

The same tendency was observed in the growth rates for the periods before and after the 56th day from the calculation of the relationship between time in days and shell length; juveniles showed different growth rates in the periods before and after the 56th day and they needed about 2 months to adapt themselves to the changes in environment. Therefore, the influence of density on the growth of juveniles was judged by using the results obtained after the 56th day.

Table 7. Mean shell length (mm) of young *Haliotis tuberculata* reared under different density conditions during 112 days. See Table 2 for definition of density.

Days \ Density	D0	D1	D2	D3	D4	D5
0	6.19	7.12	7.00	7.04	7.15	7.00
14	6.88	7.67	7.39	7.48	7.56	7.62
28	7.45	7.89	7.66	7.88	7.88	7.65
41	8.42	9.13	8.93	8.62	8.98	8.92
56	9.46	9.80	9.89	10.07	9.50	9.72
70	10.57	11.15	10.91	10.84	10.85	10.22
84	12.26	12.29	12.32	11.54	11.84	10.98
98	13.23	13.24	13.21	12.74	12.87	12.44
112	14.49	13.95	14.20	13.88	13.09	13.14

The rates of growth in shell length and body weight with different densities tended to decrease with the increase in densities as shown in Table 8 and Fig. 6. The monthly rates (%) of growth in shell length with different densities which are the most important rates to be measured were as follows; 28.5 (83/m²), 22.7 (625/m²), 23.3 (1250/m²), 20.3 (2500/m²), 20.2 (3750/m²) and 18.8 (5000/m²).

4. Discussion

Juveniles used for the experiment needed about 2 months to adapt themselves to the changes in rearing conditions. The reason for this was the disturbance caused by operations such as removal from the collectors, measurement, exposure to air during the preparation of the experiments and also the changes in the

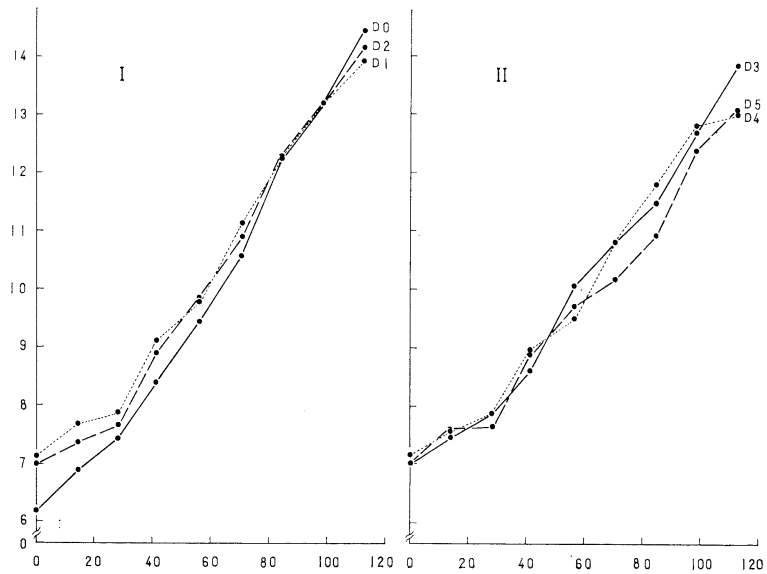

Fig. 5. Growth in shell length (ordinate, mm) of young *Haliotis tuberculata* reared under different density conditions (cf. Table 2) during 112 days (abscissa). I: Ormers reared under lower density conditions. II: Ormers reared under higher density conditions.

water current and the substrata to which they were attached, all of which took place together at the same time. In the case of mass production it is desirable to minimize the severity of these disturbances in order to obtain the best results.

From the feeding rate and efficiency values, it is concluded that *Rhodymenia*, *Ulva* and *Laminaria* in fresh forms can be used for the food of juveniles, and *Rhodymenia* is the most suitable from among these three species.

The rate of growth using mixed algae is somewhat lower than for the most effective alga used individually and this result coincides with that of SAKAI (1962). However, the ultimate benefit of a mixed food supply may be derived not only from its effect on maximization of growth but rather from other considerations such as availability of algal species in the large quantities required for mass culture. This is especially evident with regard to *Laminaria digitata*, which, although it is not of the highest food value, is most easily collected from relatively pure stands under natural condition. Moreover, it seems that the abalones feed on many species of algae in natural sea bed as suggested by INO (1952), UNO (1971) and SHEPHERD (1973). Concerning these points, it is considered that the mixed algae, mainly based on *Laminaria*, are also effective for the mass culture of young ormers.

In using the dried algae stocked as a food, another factor should be considered. It is the natural decrease rate of food in the water as shown in Table 9. From the level of the decrease rate and efficiency, it can be considered that only dried *Rhodymenia* is suitable as a

Table 8. Rate of growth in shell length and body weight of young *Haliotis tuberculata* reared under different density conditions. See Table 2 for definition of density.

Items / Density	Initial shell length (mm)	Increment of shell length (mm)	Monthly growth rate in shell length (%)	Initial body weight (mg)	Increment of body weight (mg)	Monthly growth rate in body weight (%)
D0	9.46	5.03	28.5	120.0	344.0	153.6
D1	9.80	4.15	22.7	148.0	264.5	95.6
D2	9.89	4.31	23.3	146.0	301.0	110.4
D3	10.07	3.81	20.3	158.5	267.5	90.4
D4	9.50	3.59	20.2	138.5	227.5	88.0
D5	9.72	3.42	18.8	148.5	222.5	80.3

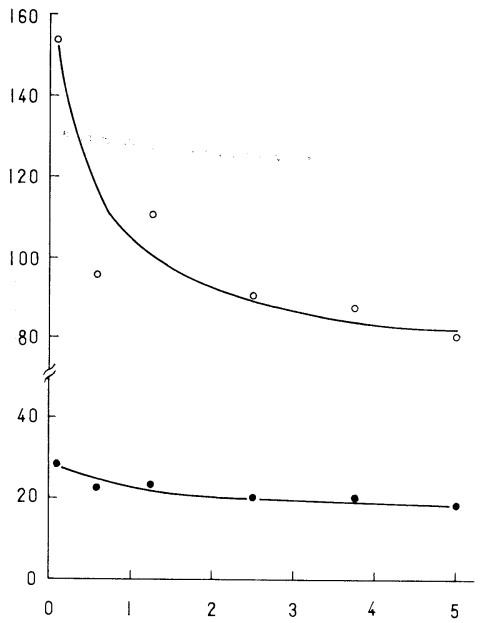

Fig. 6. Relation between the rearing density (abscissa, $\times 1000/m^2$) and the growth rate (ordinate, %) of young *Haliotis tuberculata*. Open circles, monthly growth rate in body weight; solid circles, monthly growth rate in shell length.

Table 9. Decrease in weight (mg) of foods during 48 hours in the tank without ormers for experimental control (calculated in dry weight). See Table 2 for abbreviation of food.

Items / Food		Lf	Rf	Uf	Ld	Rd	Ud	A1	A2
Initial weight	(W1)	4.6	2.9	4.2	3.8	3.95	4.1	3.7	3.7
Final weight	(W2)	3.7	2.5	4.1	1.7	2.0	2.7	0.8	2.4
Decrease of weight	(W1−W2)	0.9	0.4	0.1	2.1	1.95	1.4	2.9	1.3
Rate (%) of decrease	$\left(\frac{W1-W2}{W1}\times 100\right)$	19.6	13.8	2.4	55.3	49.4	34.1	78.4	35.1

dried alga for stocking use.

SAGARA and SAKAI (1974) reported that an artificial diet can be used as food for mass production of abalone juveniles. From the view point only of the shell length growth rate, it may be possible to say that the artificial diets tested in the present experiments can be used as food for juveniles. But in the case of mass production, the natural decrease rate should be also considered. From this point of view, it can be suggested that only the food which has a low natural decrease rate such as No. 2 (35.1 %) can be used, because foods which change and break up easily as No. 1 does cause deterioration of water quality and increase the amount of work such as the cleaning of tanks and the exchange of water. Otherwise the structure of the tanks must be designed (e.g. double bottom tanks using net cages) so as to discharge the leftover and dissolved food.

OGINO and KATO (1964) stated that abalone required protein levels of about 20 % in the artificial diet. Concerning this point, the content of protein in artificial diet No. 2 with a high food value was 21 %, and this is almost the same as Ogino's.

To determine the most suitable rearing density for mass production, the total production from a limited space and the management or operation of the rearing system must be considered. Above all, the monthly rate of shell length growth for juveniles of about 10 mm should be more than 20 %, based on the time required to reach the final shell length. In view of these considerations and the results of the present experiments, the most suitable rearing density for ormers of 7–10 mm can be considered to be between 2500/m^2–3750/m^2. Nevertheless, the actual rearing density must be decided based on the various rearing conditions such as the tank system, variation of food, initial size of juveniles and the amount of production desired, etc.

5. Summary

Tank rearing experiments with juveniles of *Haliotis tuberculata* to determine the influence of food and density on the rate of growth of juveniles were carried out during 112 days (Apr. 30–Aug. 20, 1975) at Centre Océanologique de Bretagne in Brest, France. The results are summarized as follows:

1) It is considered that after being removed from collectors, juveniles need about 2 months to adapt themselves to the changes of food and environmental conditions.

2) The effects of feeding with three species of algae in both fresh and dried conditions are as follows; the highest rates of growth were obtained with *Rhodymenia*, followed by *Ulva* and the lowest was with *Laminaria*.

3) For the stocking of a supply of food, using dried algae in mass production, only *Rhodymenia* is suitable for this use among the three species tested.

4) The rate of growth using mixed algae is somewhat lower than for the most effective alga used individually. But in case of mass culture, the food of mixed algae mainly based on *Laminaria* which is easily collected is also effective.

5) Feeding with an artificial diet composed mainly of mixed vegetable protein (extract of soya bean, dried yeast, wheat germ, and bran, etc.) produces a growth rate which is nearly equivalent to that for *Rhodymenia*, the alga of highest yield.

6) Artificial diets which can maintain their shape and quality in water over a certain period of time can be used as food for juveniles in the case of mass production.

7) A rearing density of between 2500/m^2–3750/m^2 is considered reasonable for the mass production of juveniles.

Acknowledgement

The authors wish to acknowledge the continuing guidance and encouragement of Prof. T. IWAI of Kyoto University during their study. They are also greatly indebted to Prof. Y. UNO of Tokyo University of Fisheries for suggesting this subject of research and for stimulating interest in it. Sincere thanks are due to Mr. J. J. SABAUT of G. I. E. E. R. N. A., Service Pisciculture-Aquaculture, who kindly produced the artificial diet. Finally they would like to thank Prof. K. TAKAGI, Assistant Prof. N. ISHIWATA and J. J. WALFORD, visiting researcher, of

Tokyo University of Fisheries for their kind helps in various ways.

References

INO, T. (1952): Biological studies on the propagation of Japanese abalone (Genus *Haliotis*). Bull. Tokai Reg. Fish. Res. Lab., **5**, 1-102. (In Japanese with English summary).

KIKUCHI, S. (1964): Study on the culture of abalone, *Haliotis discus hannai* INO. Cont. 1964 Peking Symp. Gen **041**, 185-202.

KIKUCHI, S., Y. SAKURAI, M. SASAKI and T. ITO (1967): Food values of certain marine algae for the growth of the young abalone, *Haliotis discus hannai*. Bull. Tohoku Reg. Fish. Res. Lab., **27**, 93-100. (In Japanese with English summary).

KOIKE, Y. (1978): Biological and ecological studies on the propagation of the ormer, *Haliotis tuberculata* LINNAEUS I. Larval development and growth of juveniles. La mer Tokyo, **16**, 124-136.

OGINO, C. and E. OHTA (1963): Studies on the nutrition of abalone—I. Feeding trials of abalone, *Haliotis discus* REEVE, with artificial diets. Bull. Jap. Soc. Sci. Fish., **29**, 691-694. (In Japanese with English summary).

OGINO, C. and N. KATO (1964): Studies on the nutrition of abalone—II. Protein requirements for growth of abalone, *Haliotis discus*. Bull. Jap. Soc. Sci. Fish., **30**, 523-526. (In Japanese with English summary).

SAGARA, J. and K. SAKAI (1974): Feeding experiment of juvenile abalones with four artificial diets. Bull. Tokai Reg. Fish. Res. Lab., **77**, 1-5. (In Japanese with English summary).

SAKAI, S. (1962): Ecological studies on the abalone, *Haliotis discus hannai* INO-I. Experimental studies on the food habit. Bull. Jap. Soc. Sci. Fish., **28**, 766-779. (In Japanese with English summary).

SHEPHERD, S. A. (1973): Studies on southern Australian abalone (Genus *Haliotis*)-I. Ecology of five sympatric species. Aust. J. mar. Freshwat. Res., **24**, 217-257.

SHIBUI, T. (1972): On the normal development of eggs of Japanese abalone, *Haliotis discus hannai* INO, and ecological and physiological studies of its larvae and youngs. Bull. Iwate Pref. Fish. Ex. St., **2**, 1-69.

TOYAMA, C., S. SATO, K. MIZUGUCHI and S. KANEKO (1975): [Influence of rearing density on the growth and survival rate of young abalones]. Bull. Chiba Pref. Fish. Ex. St., **34**, 1-11. (In Japanese).

UNO, Y. (1971): [Chapter 2, Section 4. Abalone, p. 669-703. in N. KAWAMOTO, ed., Special Fish Thremmatology]. Koseisha Koseikaku Pbl. Co., Tokyo. (In Japanese).

欧州産アワビ *Haliotis tuberculata* LINNAEUS の増殖に関する生物学的および生態学的研究

II. 稚貝の成長に関する餌料と飼育密度の影響

小池康之，ジャン－ピエール・フラッシュ，ジョゼフ・マズリエ

要旨：採苗後4カ月目（殻長約7mm）の稚貝の成長に関する餌料および飼育密度の影響を明らかにする目的で112日間飼育実験を行ない，次の結果を得た。

コレクターから剝離後の稚貝は飼育環境および餌料転換に対する適応に約2カ月を要するものと考えられる。

実験に供した3種類の海藻の餌料価値は，*Rhodymenia palmata* が最も高く，*Ulva lactuca* がこれに次ぎ，*Laminaria digitata* が最も低い。稚貝量産における乾燥海藻の貯蔵利用には *Rhodymenia* が適している。混合投与による餌料効果は単独投与による優位な海藻よりも多少劣る。

海水中における保形性が良好であれば，人工餌料による稚貝の量産飼育は可能である。

稚貝の量産飼育における適正飼育密度は，2500/m^2～3750/m^2 と推定される。

学 会 記 事

1. 昭和53年12月１日，東京水産大学において，編集委員会が開かれ，第16巻３号の編集が行われた。

2. 昭和53年12月25日，東京水産大学において，第２回学会賞受賞候補者推薦委員会が開かれ，審議の結果，昭和54年度受賞候補者として，井上実氏を推薦することとし，この旨石野委員長から，会長に報告した。

3. 新入会員

氏　名	所　属	紹介者
石井　丈夫	東大・海洋研	丸茂　隆三

4. 賛助会員　東京工材㈱　溝口哲夫氏は，昭和54年１月11日，逝去されました。御冥福を御祈りいたします。

5. 交換及び寄贈図書

1) 海洋技術と法　㈶日本海洋協会
2) 季刊　海洋時報　第11号
3) 鯨研通信　第319～321号
4) 自然（特集　理化学研究所60年のあゆみ）
5) 英国産業ニュース　11～2 月号
6) 研究実用化報告　27（10, 11, 12）
7) 海洋産業研究資料　9（7, 8, 9）
8) 航海用語集
9) 日本プランクトン学会報　25(2)
10) 農業土木試験場報告　第17号
11) 国立科学博物館研究報告（A類）　4(4)
12) なつしま　第34～38号
13) 横須賀市博物館研究報告　第25号
14) 横須賀市博物館資料集　第２号
15) 広島大学水畜産学部紀要　17(2)
16) 千葉県水産試験場研究報告　第37号
17) 国立博物館専報　第11号
18) Cruise Report / 海洋地質図　No. 10, 11
19) la gazette　N° 23, 24
20) Revue des Travaux de l'Institut des Péches Maritimes　Tome XLI Fasc 1, 2
21) Bulletin d'Information　N° 117～119
22) 30th Anniversary Commemorative Research Study Compilation　1978. 11
23) American Museum Novitates　No. 2642
24) Annales Hydrographiques　6(1)

日仏海洋学会役員

顧　問　ユベール・ブロッシェ　ジャン・デルサルト　ジャック・ロベール　アレクシス・ドランデール　ベルナール・フランク

名誉会長　ミシェル・ルサージェ

会　長　佐々木忠義

副会長　黒木敏郎，國司秀明

常任幹事　阿部友三郎，宇野　寛，永田　正

庶務幹事　三浦昭雄

編集幹事　有賀祐勝

幹　事　石野　誠，井上　実，今村　豊，岩下光男，川原田　裕，神田献二，菊地真一，草下孝也，斎藤泰一，佐々木幸康，杉浦吉雄，高木和徳，高野健三，辻田時美，奈須敬二，根本敬久，半沢正男，松生　洽，丸茂隆三，森田良美，山中鷹之助　（五十音順）

監　事　久保田　穣，岩崎秀人

評議員　青山恒雄，赤松秀雄，秋山　勉，阿部宗明，阿部友三郎，新崎盛敏，有賀祐勝，石野　誠，石渡直典，市村俊英，井上　実，今村　豊，入江春彦，岩崎秀人，岩下光男，岩田憲幸，宇田道隆，宇野　寛，大内正夫，小倉通男，大村秀雄，岡部史郎，岡見　登，梶浦欣二郎，加藤重一，加納　敬，川合英夫，川上太左英，川村輝良，川原田　裕，神田献二，菊地真一，草下孝也，楠　宏，国司秀明，久保田　穣，黒木敏郎，小泉政美，小林　博，小牧勇蔵，西条八束，斎藤泰一，斎藤行正，佐伯和昭，坂本市太郎，佐々木忠義，佐々木幸康，猿橋勝子，柴田恵司，下村敏正，庄司大太郎，杉浦吉雄，関　文威，多賀信夫，高木和徳，高野健三，高橋淳雄，高橋　正，谷口　旭，田畑忠司，田村　保，千葉卓夫，辻田時美，寺本俊彦，鳥羽良明，冨永政英，鳥居鉄也，中井甚二郎，中野猿人，永田　正，永田　豊，奈須敬二，奈須紀幸，西沢　敏，新田忠雄，根本敬久，野村　正，半沢正男，半谷高久，樋口明生，菱田耕造，日比谷　京，平野敏行，深沢文雄，深瀬　茂，福島久雄，淵　秀隆，星野通平，増沢穣太郎，増田辰良，松生　洽，松崎卓一，丸茂隆三，三浦昭雄，三宅泰雄，宮崎千博，宮崎正衛，村野正昭，元田　茂，森川吉郎，森田良美，森安茂雄，安井　正，柳川三郎，山路　勇，山中鷹之助，山中一郎，山中　一，吉田多摩夫，渡辺精一　（五十音順）

マルセル・ジュグラリス，ジャン・アンクティル，ロジェ・ペリカ

賛助会員

旭化成工業株式会社	東京都千代田区有楽町 1-1-2　三井ビル
株式会社内田老鶴圃新社　内田悟	東京都千代田区九段北 1-2-1　蜂谷ビル
株式会社　オーシャン・エージ社	東京都千代田区神田美土代町 11-2　第1東英ビル
株式会社　大林組	東京都千代田区神田司町 2-3
小樽舶用電機株式会社	小樽市色内町 3-4-3
株式会社オルガノ	東京都文京区本郷 5-5-16
株式会社　海洋開発センター	東京都港区赤坂 1-9-1
社団法人　海洋産業研究会	東京都港区新橋 3-1-10　丸藤ビル
協同低温工業株式会社	東京都千代田区神田佐久間町 1-21　山伝ビル
協和商工株式会社	東京都豊島区目白 4-24-1
小松川化工機株式会社	東京都江戸川区松島 1-342
小山康三	東京都文京区本駒込 6-15-10　英和印刷社
三信船舶電具株式会社	東京都千代田区神田 1-16-8
三洋水路測量株式会社	東京都港区新橋 5-23-7　三栄ビル
シュナイダー財団極東駐在事務所	東京都港区南青山 2-2-8　DF ビル
昭和電装株式会社	高松市寺井町 1079
新日本気象海洋株式会社	東京都渋谷区東 1-19-3　青山ビル
株式会社鶴見精機	横浜市鶴見区鶴見町 1506
東亜建設工業株式会社	東京都千代田区四番町 5
株式会社東京久栄	東京都中央区日本橋 3-1-15　久栄ビル
東京製綱繊維ロープ株式会社	東京都中央区日本橋室町 2-6　江戸ビル
株式会社東邦電探	東京都杉並区宮前 1-8-9
中川防蝕工業株式会社	東京都千代田区神田鍛冶町 2-2-2　東京建物ビル
株式会社　ナック	東京都港区西麻布 1-2-7　第17興和ビル
日本アクアラング株式会社	神奈川県厚木市温水 2229-4
日本海洋産業株式会社	東京都新宿区西新宿 2-6-1　新宿住友ビル
日本テトラポッド株式会社	東京都港区新橋 2-1-13　新橋富士ビル9階
社団法人　日本能率協会	東京都港区芝公園 3-1-22　協立ビル
日本プレスコンクリート株式会社	東京都中央区日本橋本石町 1-4
深田サルベージ株式会社	東京都千代田区神田錦町 1-9-1　天理教ビル8階
藤田潔	東京都新宿区四谷 3-9　光明堂ビル　株式会社ビデオプロモーション
藤田峯雄	東京都江東区南砂 1-3-25　株式会社 中村鉄工所
フランス物産株式会社	東京都千代田区神田小川町 3-20-2　増淵ビル
古野電気株式会社	東京都中央区八重洲 4-5　藤加ビル
丸文株式会社	東京都中央区日本橋大伝馬町 2-1-1
三井海洋開発株式会社	東京都千代田区霞ケ関 3-2-5　霞ケ関ビル3002号室
宮本悟	東京都中央区かちどき 3-3-5　かちどきビル　㈱ 本地郷
吉野計器製作所	東京都北区西ケ原 1-14
株式会社離合社	東京都千代田区神田鍛冶町 1-10-4
株式会社渡部計器製作所	東京都文京区向丘 1-7-17

長期捲自記流速計

(NC-Ⅱ)

本流速計は海中に設置し、内蔵した記録器に流速流向を同時に記録するプロペラ型の流速計で約20日間の記録を取る事が出来ます。但し流速は20分毎に3分間の平均流速を又流向は20分毎に一回、共に棒グラフ状に記録しますから読取が非常に簡単なのが特徴となって居ります。

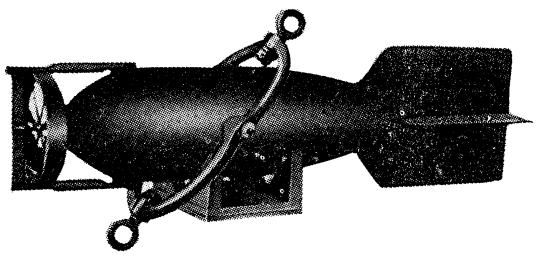

(外器)

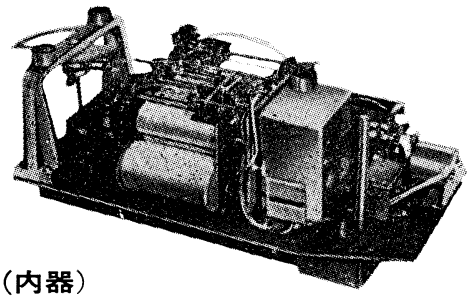

(内器)

プロペラはA，B，C三枚一組になって居り

A(弱流用)……1m/sec
B(中流用)……2m/sec
C(強流用)……3m/sec

} 迄で一枚毎に検定してあります。

弱流ペラーに依る最低速度は約4cm/secです。

フース型長期捲自記検潮器

(LFT-Ⅲ)

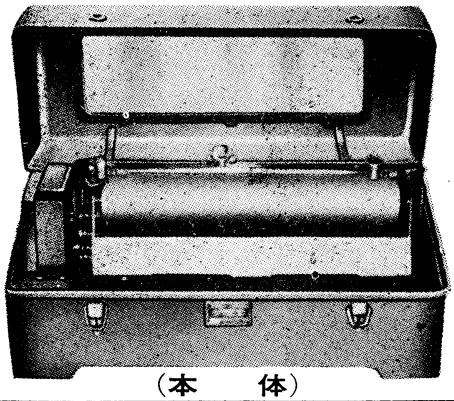

(本　体)

営業品目

階段抵抗式波高計
ケーブル式波高計
フース型検潮器
小野式自記流速計
自記水位計
港施型土圧計
理研式水中カメラ
その他海洋観測諸計器

協和商工株式会社

東京都豊島区目白4丁目24番地1号
TEL (952) 1376代表　〒171

東京支社住所変更 「関東支社：〒243 神奈川県厚木市温水 2229-4 TEL 0462-47-3222」

昭和 54 年 2 月 25 日 印刷
昭和 54 年 2 月 28 日 発行

う み

第 17 巻
第 1 号

定価 ¥950

編集者 冨永政英
発行者 佐々木忠義
発行所 日仏海洋学会
財団法人 日仏会館内
東京都千代田区神田駿河台2-3
郵便番号:101
電話:03(291)1141
振替番号:東京96503

印刷者 小山康三
印刷所 英和印刷社
東京都文京区本駒込 6-15-10
郵便番号:113
電話:03(941)6500

第 17 巻　第 1 号

目　次

Tome 17　N° 1

SOMMAIRE